Electronic Supplementary Material (ESI) for Journal of Materials Chemistry A.

Supporting Information

Energy-Efficient UV-to-NIR Active Smart Electrochromic Tetrabenzofluorene Molecules

Panichiyil V. Navya[a] and Srinivasan Sampath*[a]

[a]Panichiyil V. Navya and Srinivasan Sampath
Department of Materials Science, School of Technology,
Central University of Tamil Nadu,
Thiruvarur, India 610005
E-mail: srinivasansampath@cutn.ac.in and sampathsrinivasan@yahoo.com

Table of Contents

Section A. Experimental Procedures

Reagents and Materials

9-Bromophenanthrene, recrystallized iodine, 2-ethylhexyl bromide, 2-thienyl boronic acid pinacol ester, and 5-acetyl-2-thienyl boronic acid were purchased from Sigma Aldrich. Trifluoroacetic acid, tetrakis(triphenylphosphine)palladium(0), and 3-thienyl boronic acid were procured from TCI chemicals. Methyl formate, magnesium turnings, *N*-bromosuccinimide, triethylamine, potassium iodide, potassium hydroxide, anhydrous sodium sulfate, silica gel (100−200 mesh) and tetrahydrofuran, *N*, *N*-dimethylformamide, and dimethyl sulfoxide were obtained from Avra. Hexane, ethanol, ethyl acetate, diethyl ether, dichloromethane, chloroform, were obtained from Merck, India and used without further purification. ITO (Transparent Conductive Glass Slide; Resistivity - 10 ohms/sq; Size: 50mm×25mm×1.1mm; HSN:70200019) plates were purchased from Shilpa Enterprises, Amazon Seller Services, India.

Characterization

NMR spectra were recorded with a Bruker DRX Spectrometer (^{1}H NMR-400 MHz and ^{13}C NMR-100 MHz) and chemical shifts (δ) were determined using tetramethylsilane (TMS) as the internal standard. The ATR-FTIR spectra were recorded using the PerkinElmer spectrum 2 spectrometer in the range 4000 – 400 cm^{-1}. UV–visible spectra were recorded on JASCO V-770 spectrophotometer and emission spectra were recorded on HITACHI f-4700 fluorescence spectrophotometer. The life-time measurements were carried out on HORIBA FluoroMax c$^+$ TCsPC DeltaHub. Mass analysis was performed on a High-Resolution Liquid Chromatograph Mass Spectrometer (HRLCMS) Agilent Technologies (1290 Infinity UHPLC System,1260 infinity Nano HPLC with Chipcube, 6550 iFunnel Q-TOFs). TG/DTA 6200 (SEIKO) thermal analyzer was used to perform thermogravimetric analysis (TGA) with a heating rate of 10 °C min^{-1} under ambient atmosphere in the temperature range of 25 − 700 °C. Electrochemical experiments were carried out on CHI660E electrochemical workstation. The electrochemical cell contained a glassy carbon electrode as working electrode, Pt wire as the counter electrode and calomel electrode as the reference electrode in DCM using 0.1 M $TBAPF_6$ as the supporting electrolyte at a scan rate at various scan rates. Spectroelectrochemical experiments were performed with an electrolytic cell composed of a 1 mm path length electrochromic cuvette, Ag/Ag^+ quasi reference electrode, platinum mesh and a platinum wire were used as the working electrode and the counter electrode, respectively. The spectroelectrochemical cell was filled with DCM solutions of each compound and $TBAPF_6$ (0.1 M). UV–vis–NIR spectra were recorded using DH-2000-BAL Light Source and FLAME-S-XR1-ES as the detector. The potential was supplied by means of an CH Electrochemical Analyzer. Measurements were performed at 25 °C. The density functional theory (DFT) calculations were carried out with a basis set 6-31G** for all the atoms. The stationary points were fully characterized via analytical frequency calculations to confirm as either minima (all positive eigenvalues) or transition states (one imaginary eigenvalue). All geometries are fully optimized in the DFT level with B3LYP method including Grimme's-D3 empirical dispersion corrections using Gaussian16 program.

Section B. Synthetic Procedure

Compound **1** was synthesized by following the known literature procedure[1,2] starting from 9-bromophenathrene.

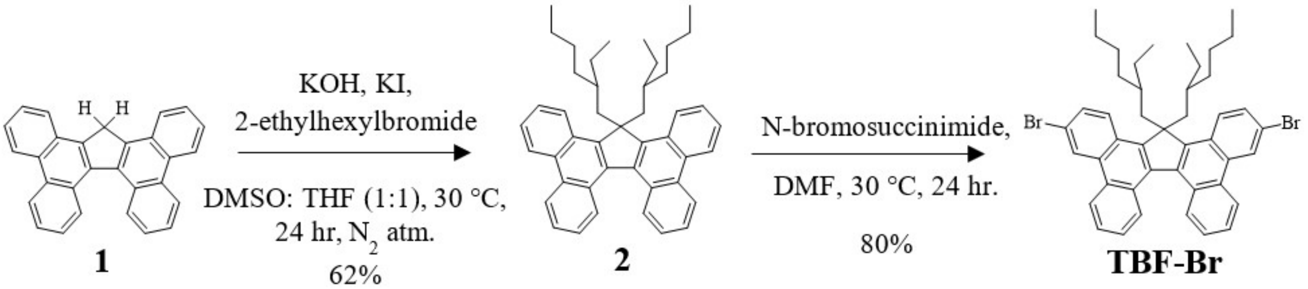

Synthesis of 2: Compound 1 (250 mg, 0.68 mmol) was taken in a 250 mL round bottom (RB) flask, a 1:1 mixture of DMSO:THF (10:10 mL) was added into it and stirred for 10 minutes under nitrogen atmosphere, followed by the addition of KOH (4.4 mmol, 247 mg) and KI (3.7 mmol, 62 mg). the reaction contents were stirred for another 10 minutes and then 2-ethylhexyl bromide (17 mmol, 0.3 mL) was added slowly and stirred under N_2 for 24 at 30 °C. The product formation was confirmed by checking the TLC and the THF was evaporated using rotary evaporator under reduced pressure. Distilled water was added into the reaction mixture and extracted using chloroform, organic layer was separated, washed many times with water, dried over Na_2SO_4 and concentrated. The final product is purified by column chromatography using pure hexane over silica gel (100-200 mesh). Yield= 62 %.

Synthesis of TBF-Br: The compound 2 (1g, 1.9 mmol) was taken in a 250 mL RB flask and dissolved 100 mL *N*, *N*- dimethylformamide (DMF). To this, *N*-Bromosuccinimide (4.2 mmol, 0.73 g) was added and stirred for 24 h at room temperature (30 °C). the completion of reaction was monitored by checking TLC, chloroform was added into the reaction content, water soluble contents are removed from the organic layer by washing the organic fraction with water. The organic layer is finally extracted, dried over anhydrous Na_2SO_4 and concentrated. The purification was done by column chromatography using pure hexane over silica gel (100-200 mesh). Yield= 80 %.

General Procedure for the Synthesis of TBFT1-3:
The dibromo derivative of tetrabenzofluorene (**TBF-Br**) (333.61 mmol, 250 mg), boronic acid (834.02 mmol), and a catalytic amount of tetrakis(triphenylphospshine)palladium(0) ([$Pd(PPh_3)_4$]) (10 mg) were taken in a pre-heated 2-neck round bottom flask, and placed in a preheated (50 °C) oil bath. The air inside the setup was replaced by nitrogen gas, followed by the addition of 13 mL dry THF, and again purged for 10 minutes. To this, 7 mL of 2 M K_2CO_3 solution is added slowly and heated to 80 °C with constant stirring under a nitrogen atmosphere for 48 h. After checking the completion of the reaction by TLC, dichloromethane was added to the reaction mixture, followed by the addition of water, and the organic layer was separated, washed many times with water, dried over anhydrous Na_2SO_4, and concentrated. Column chromatography was done with hexane: ethyl acetate by gradually increasing the polarity of the solvent over silica gel (100-200 mesh).

TBFT1: The compound TBF-T1 was obtained as pale-yellow solid; Yield = 75%; m.p. = 128-130 °C. ^{1}H NMR (400 MHz, $CDCl_3$, TMS) δ= 9.06 (m, 2H), 8.88-8.83 (m, 2H), 8.57-8.50 (m, 4H), 7.97-7.94 (d, J = 12 Hz, 2H), 7.73-7.67 (m, 6H), 7.61-7.56 (d, 2H), 7.52-7.49 (m, 2H), 2.80 (s, 4H), 1.05-0.02 (m, 30H); ^{13}C NMR ($CDCl_3$, 100 MHz) δ= 146.88, 142.69, 136.70, 132.79, 132.73, 132.67, 131.35, 131.13, 128.39, 127.60, 126.54, 125.77, 125.27, 125.12, 125.07, 123.45, 121.22, 120.59, 60.99, 44.56, 35.67, 27.76, 22.37, 13.62; FTIR (ATR): ν = 2958, 2923, 2855, 1582, 1500, 1441, 1403, 1377, 1192, 1085, 1042, 868, 826, 755, 738, 651, 597; ESI MS m/z: $[M]^+$ calcd for $C_{53}H_{54}S_2$, 754.3667; found, 754.3664.

TBFT2: The product was obtained as a yellow color solid; Yield = 85 %; m.p. = 118-120 °C. ^{1}H NMR (400 MHz, $CDCl_3$, TMS) δ= 9.08-9.06 (m, 2H), 8.88-8.83 (m, 2H), 8.56-8.48 (m, 4H), 7.99-7.96 (m, 2H), 7.74-7.68 (m, 2H), 7.62-7.57 (m, 4H), 7.40-7.38 (d, J = 8 Hz, 2H), 7.22-7.18 (t, J = 4 Hz, 2H), 2.80 (s, 4H), 0.9-0.03 (m, 30H); ^{13}C NMR ($CDCl_3$, 100 MHz) δ= 146.92, 146.84, 144.92, 136.85, 136.78, 131.36, 131.21, 128.55, 128.32, 127.59, 125.89, 125.39, 125.32, 125.11, 124.45, 123.50, 123.43, 120.69, 60.95, 44.56, 35.67, 27.82, 22.36, 13.58; FTIR (ATR): ν = 2957, 2924, 2853, 1582, 1536, 1500, 1457, 1443, 1378, 1259, 1228, 1081, 1043, 880, 853, 816, 757, 688, 616, 565; ESI MS m/z: $[M]^+$ calcd for $C_{53}H_{54}S_2$, 754.3667; found, 754.3669.

TBFT3: The product was a brown color solid; Yield = 57 %; ^{1}H NMR (400 MHz, $CDCl_3$, TMS) δ= 9.15-9.13 (m, 2H), 8.87-8.83 (m, 2H), 8.56-8.51 (m, 4H), 8.02-7.98 (m, 2H), 7.79-7.77 (d, J = 4 Hz, 2H), 7.77-7.72 (m, 2H), 7.64-7.60 (m, 4H), 2.80 (s, 4H), 2.64 (s, 6H), 0.92-0.08 (m, 30H); ^{13}C NMR ($CDCl_3$, 100 MHz) δ= 190.66, 153.22, 146.90, 143.21, 143.16, 137.64, 133.73, 133.19, 130.27, 129.40, 127.61, 126.32, 126, 125.64, 125.56, 124.26, 124.15, 123.48, 121.5, 61.2, 44.56, 35.73, 26.65; FTIR (ATR): ν = 2957, 2922, 2855, 1659, 1533, 1451, 1434, 1356, 1271, 1082, 1029, 924, 877, 833, 800, 755, 656, 607, 572; ESI MS m/z: $[M{+}H]^+$ calcd for $C_{57}H_{59}O_2S_2$, 839.3956; found, 839.3949.

Section C. NMR studies of TBFT1

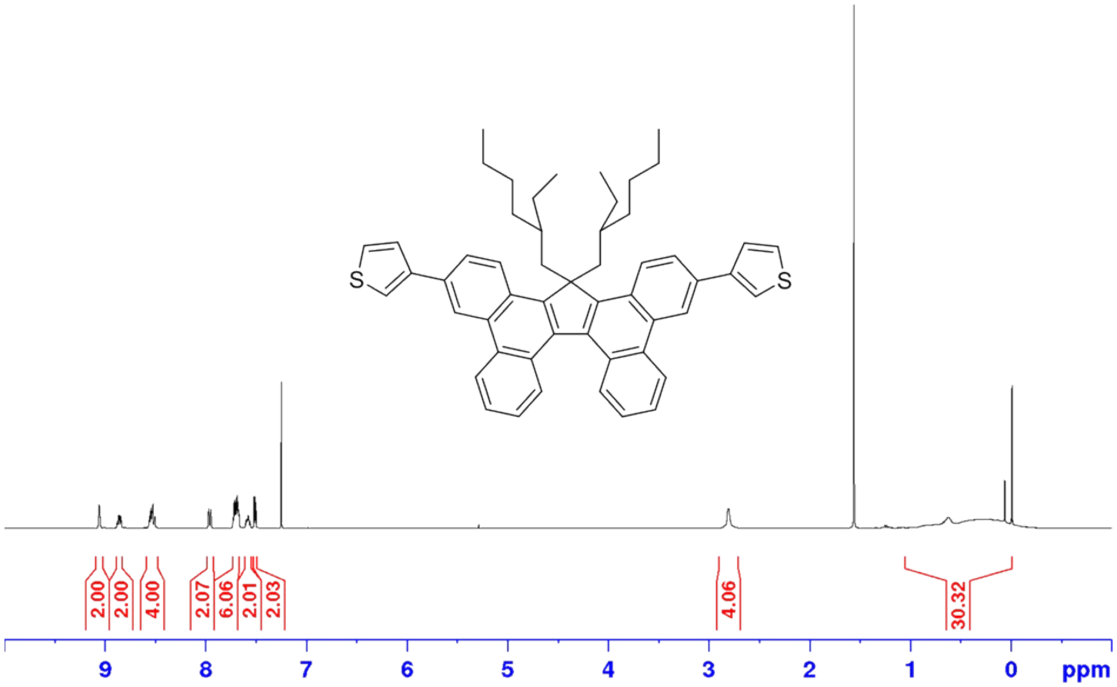

Figure S1. ^{1}H NMR spectrum of TBFT1 in $CDCl_3$ at 298 K.

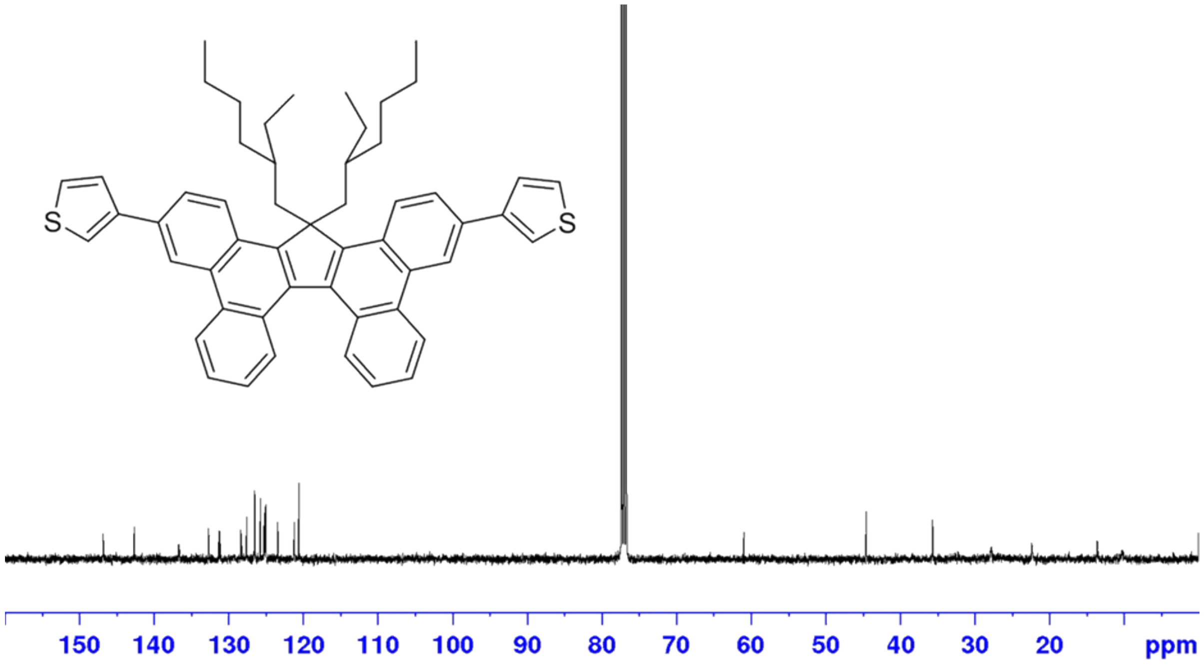

Figure S2. ^{13}C NMR spectrum of TBFT1 in $CDCl_3$ at 298 K.

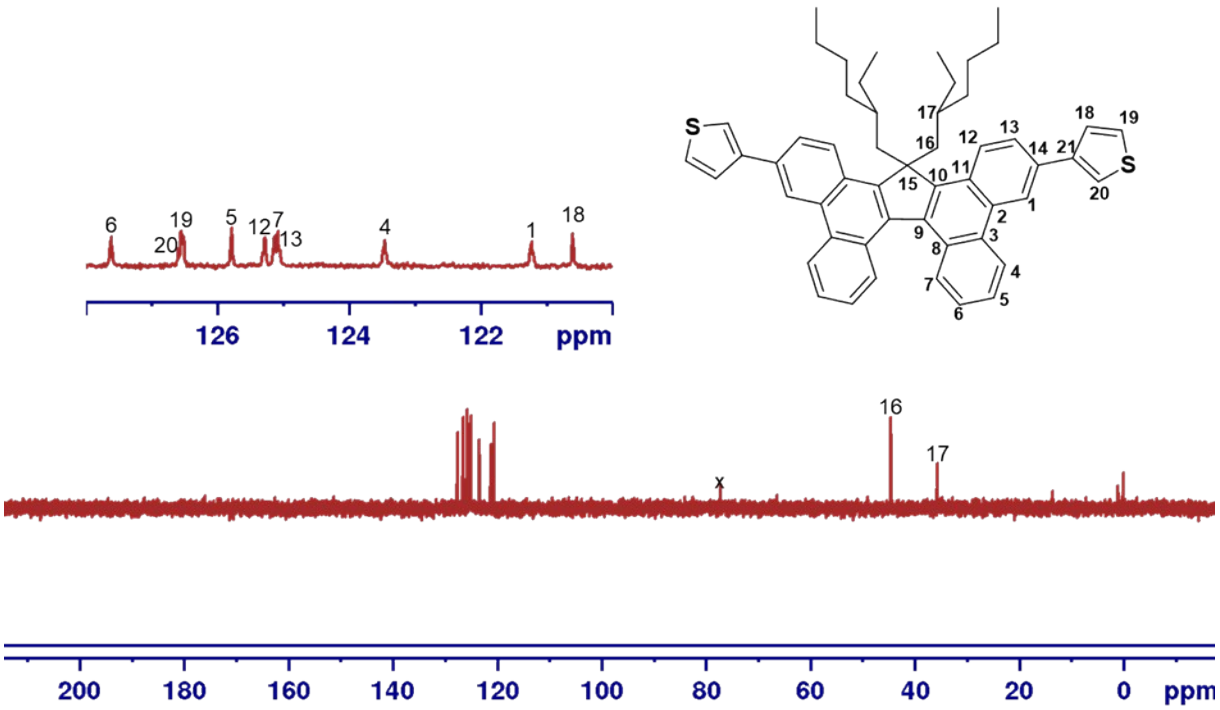

Figure S3. DEPT 45 of TBFT1 in $CDCl_3$ at 298 K.

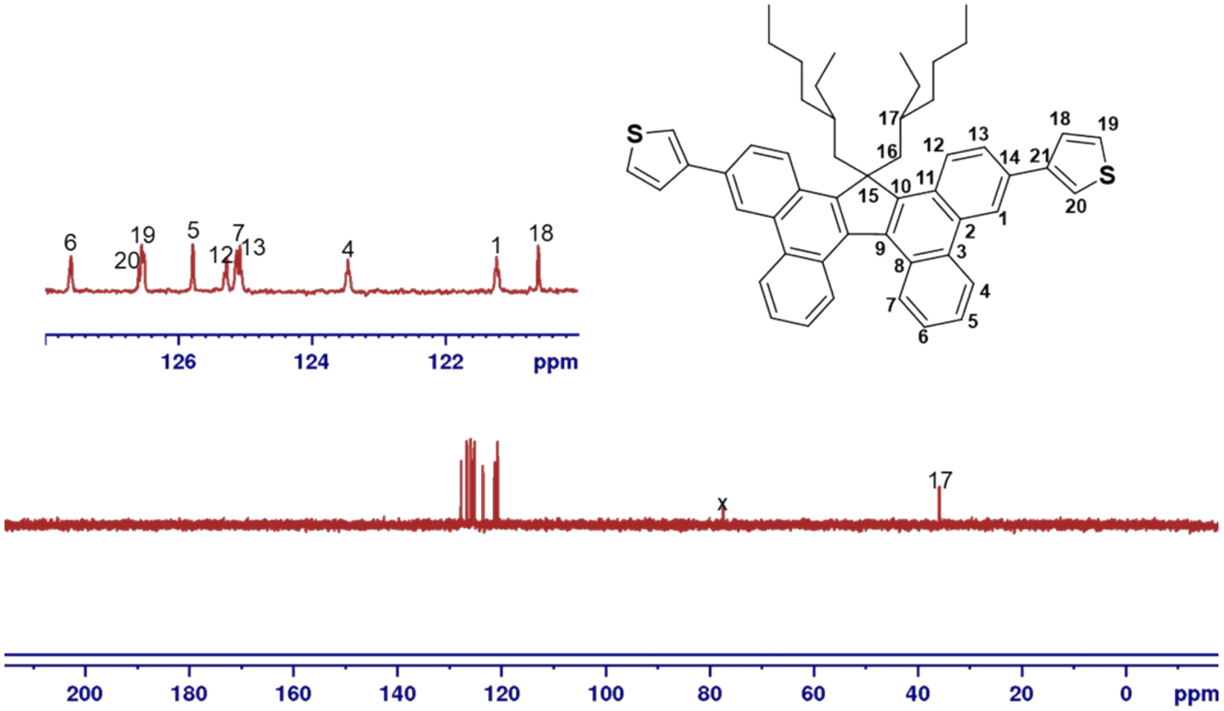

Figure S4. DEPT 90 of TBFT1 in $CDCl_3$ at 298 K.

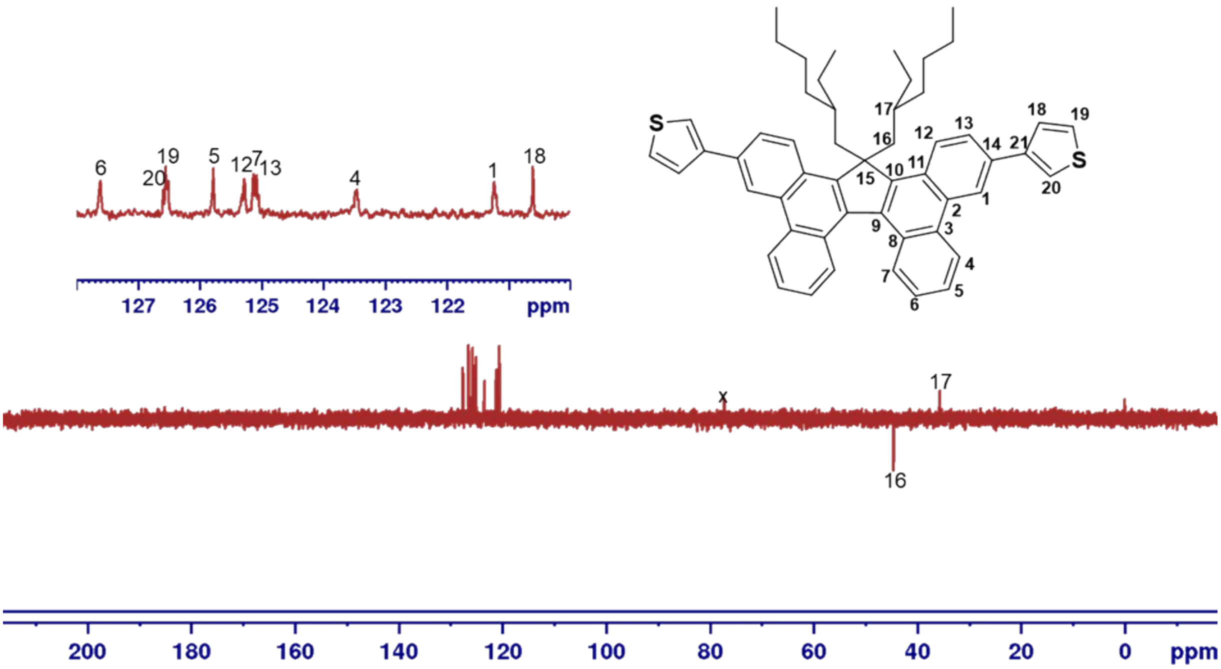

Figure S5. DEPT 135 of TBFT1 in $CDCl_3$ at 298 K.

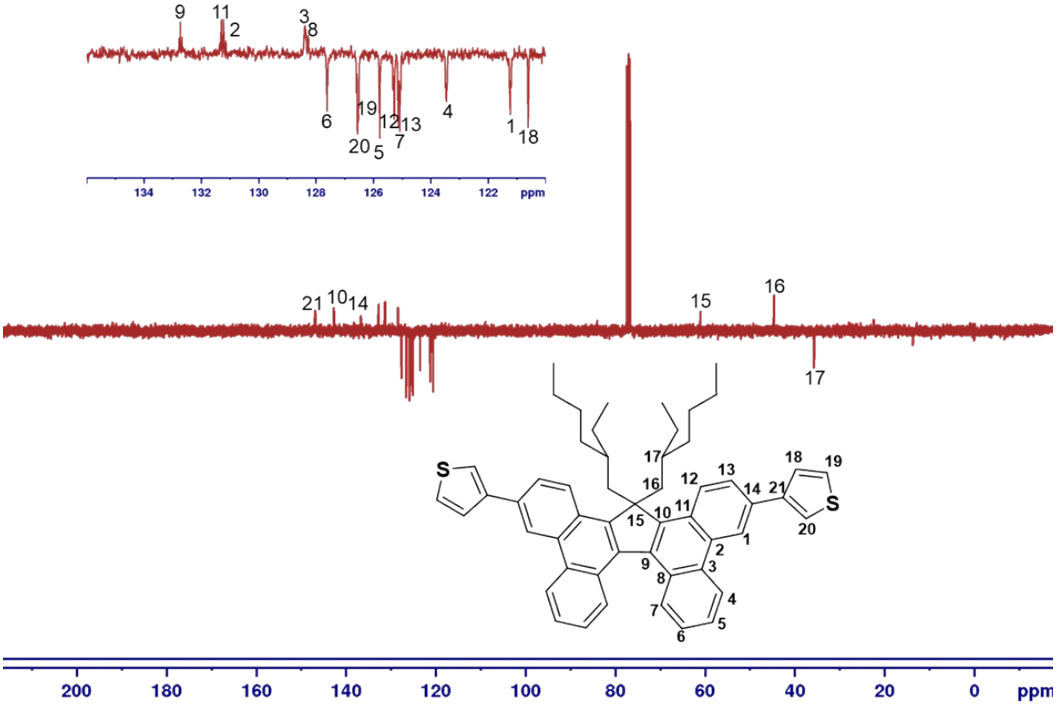

Figure S6. JMOD of TBFT1 in $CDCl_3$ at 298 K.

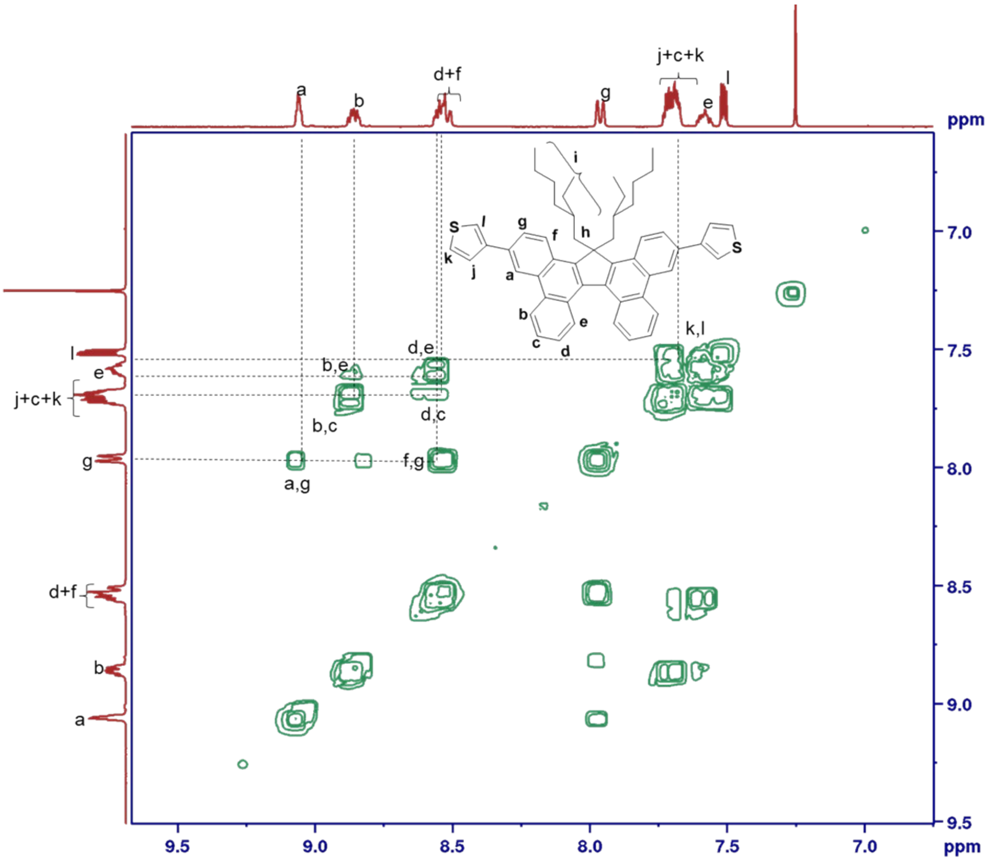

Figure S7: ^{1}H-^{1}H COSY spectrum of TBFT1 in $CDCl_3$ at 298 K.

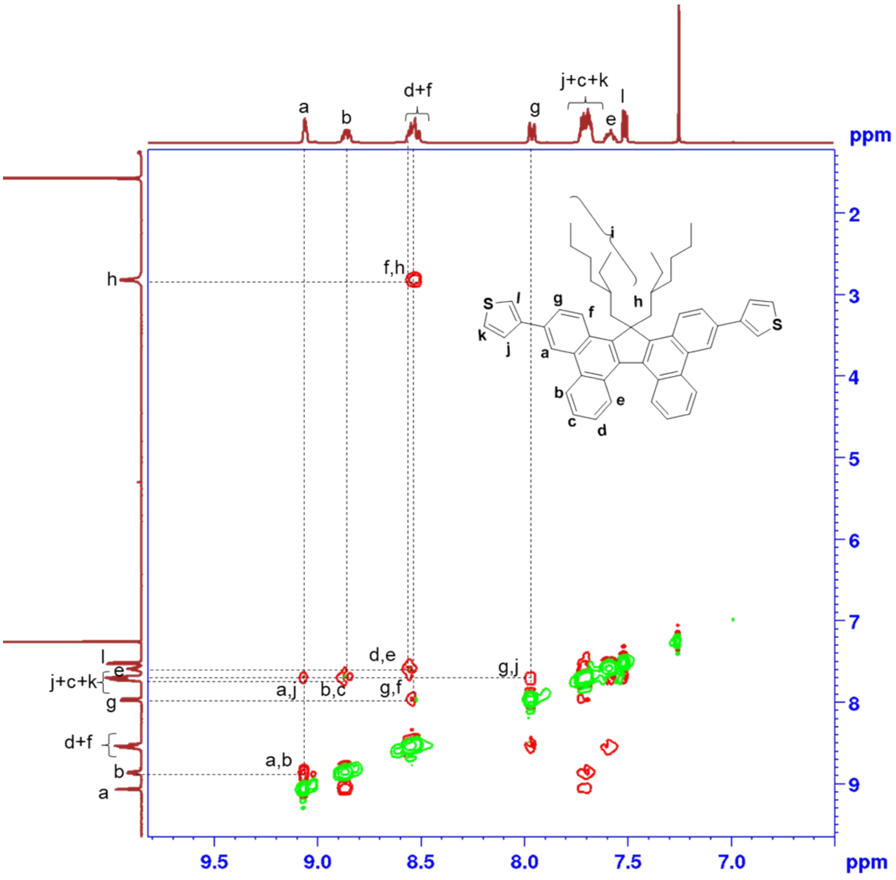

Figure S8: ^{1}H-^{1}H NOESY spectrum of TBFT1 in $CDCl_3$ at 298 K.

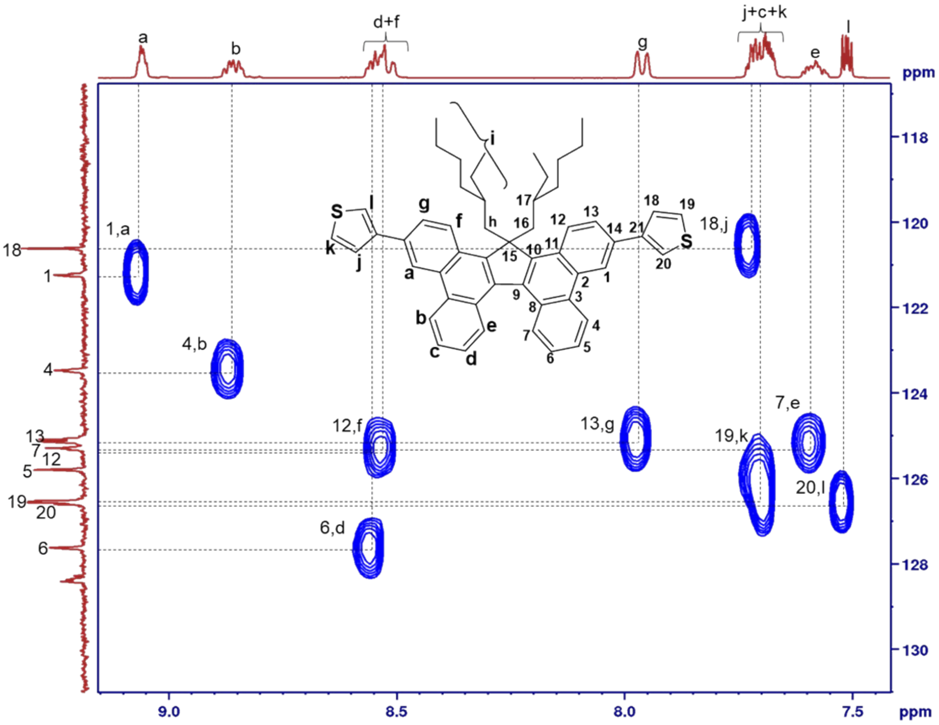

Figure S9: ^{1}H-^{13}C HSQC spectrum of TBFT1 in CDCl$_3$ at 298 K.

Section D. NMR studies of TBFT2

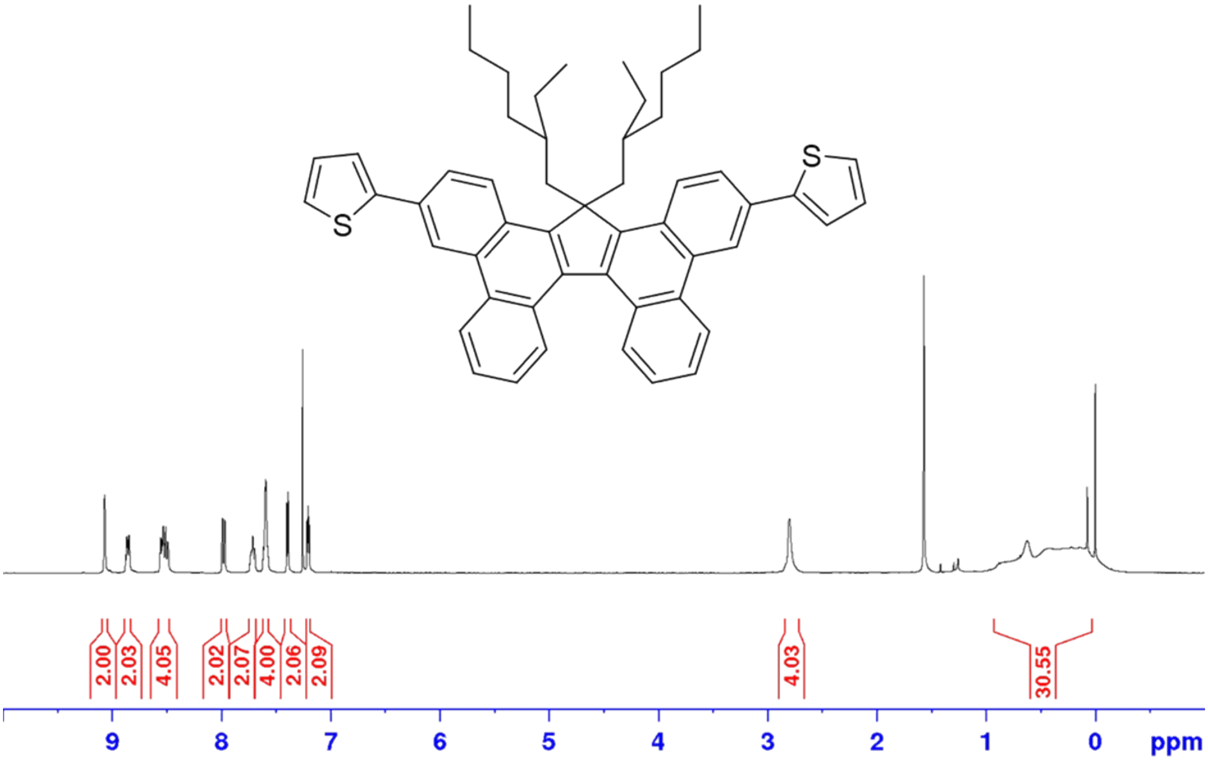

Figure S10. ^{1}H NMR spectrum of TBFT2 in CDCl$_3$ at 298 K.

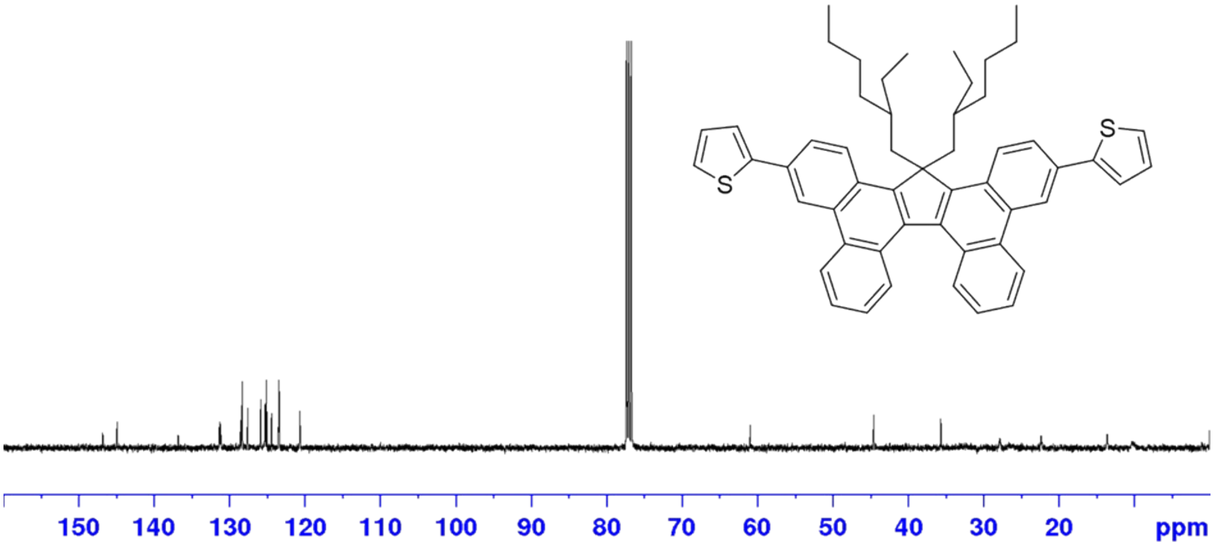

Figure S11. ^{13}C NMR spectrum of TBFT2 in $CDCl_3$ at 298 K.

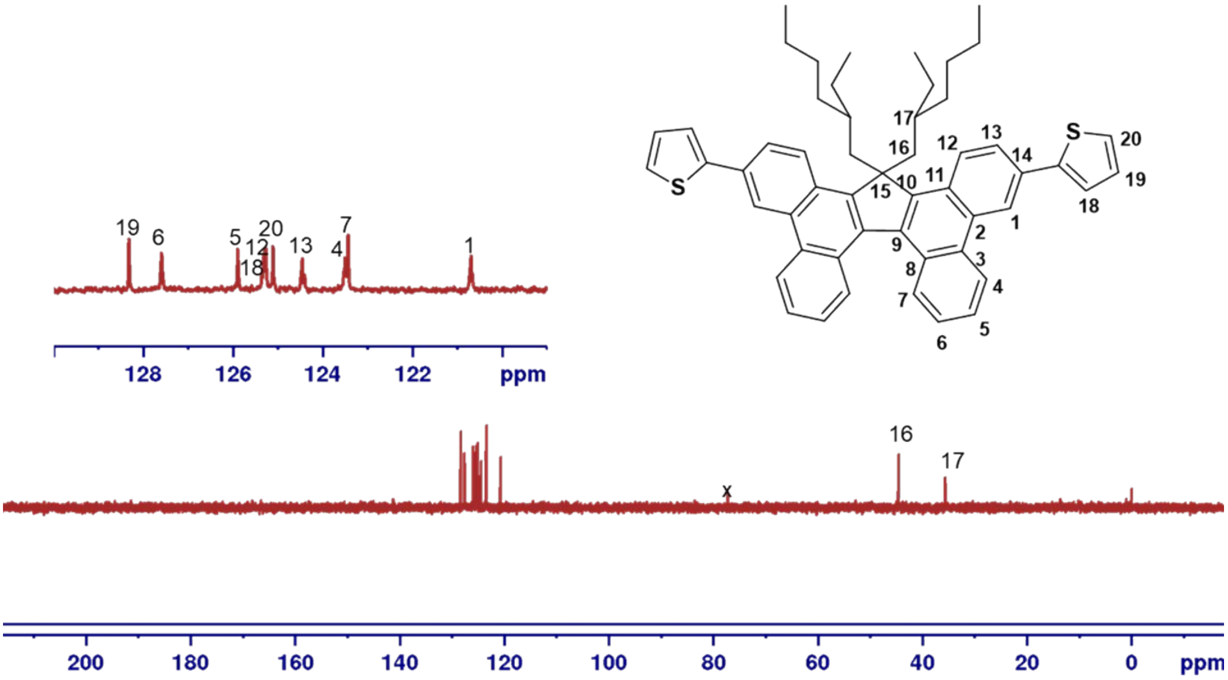

Figure S12. DEPT 45 of TBFT2 in $CDCl_3$ at 298 K.

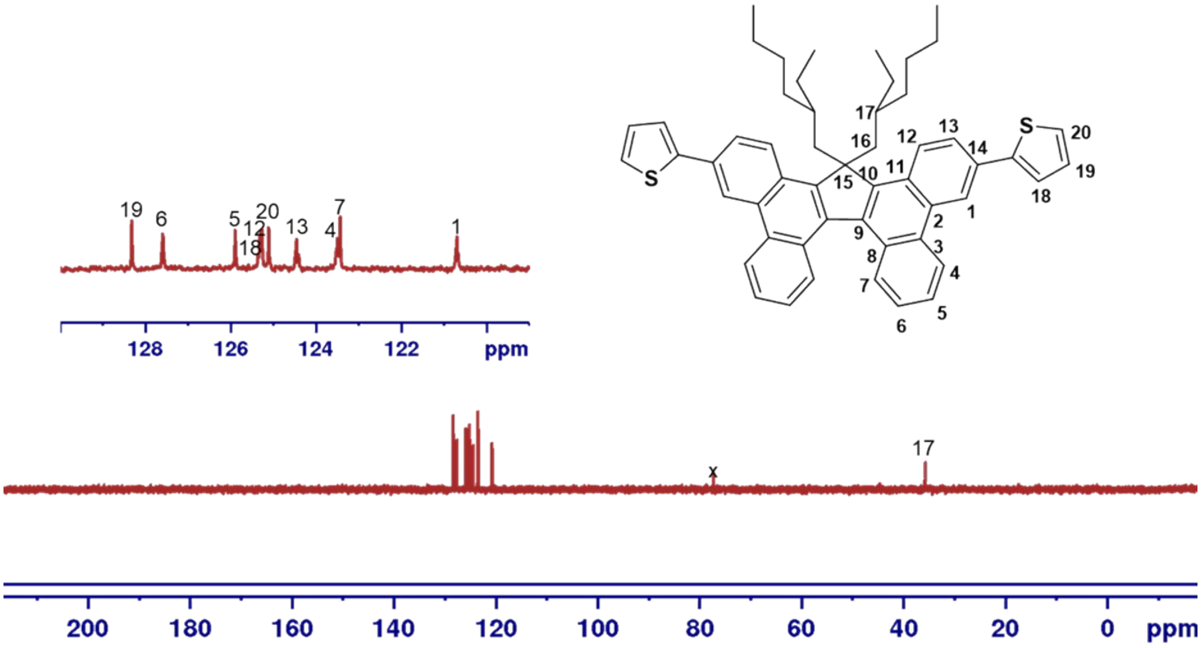

Figure S13. DEPT 90 of TBFT2 in $CDCl_3$ at 298 K.

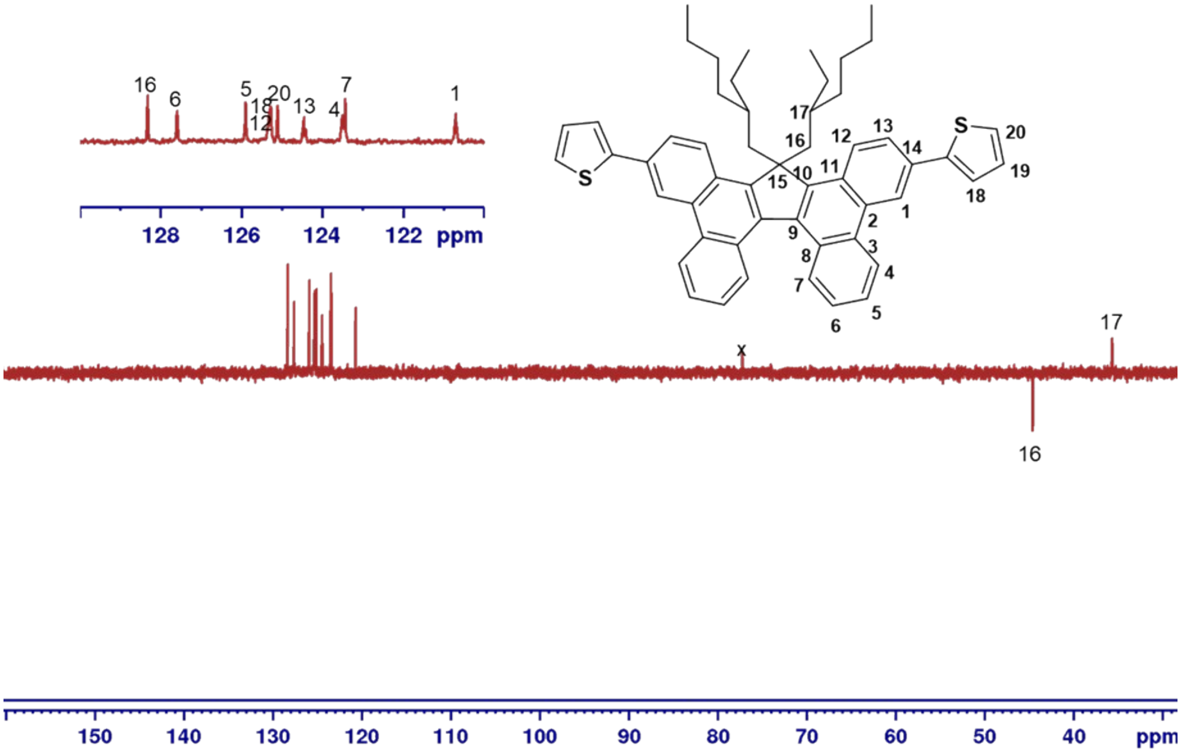

Figure S14. DEPT 135 of TBFT2 in $CDCl_3$ at 298 K.

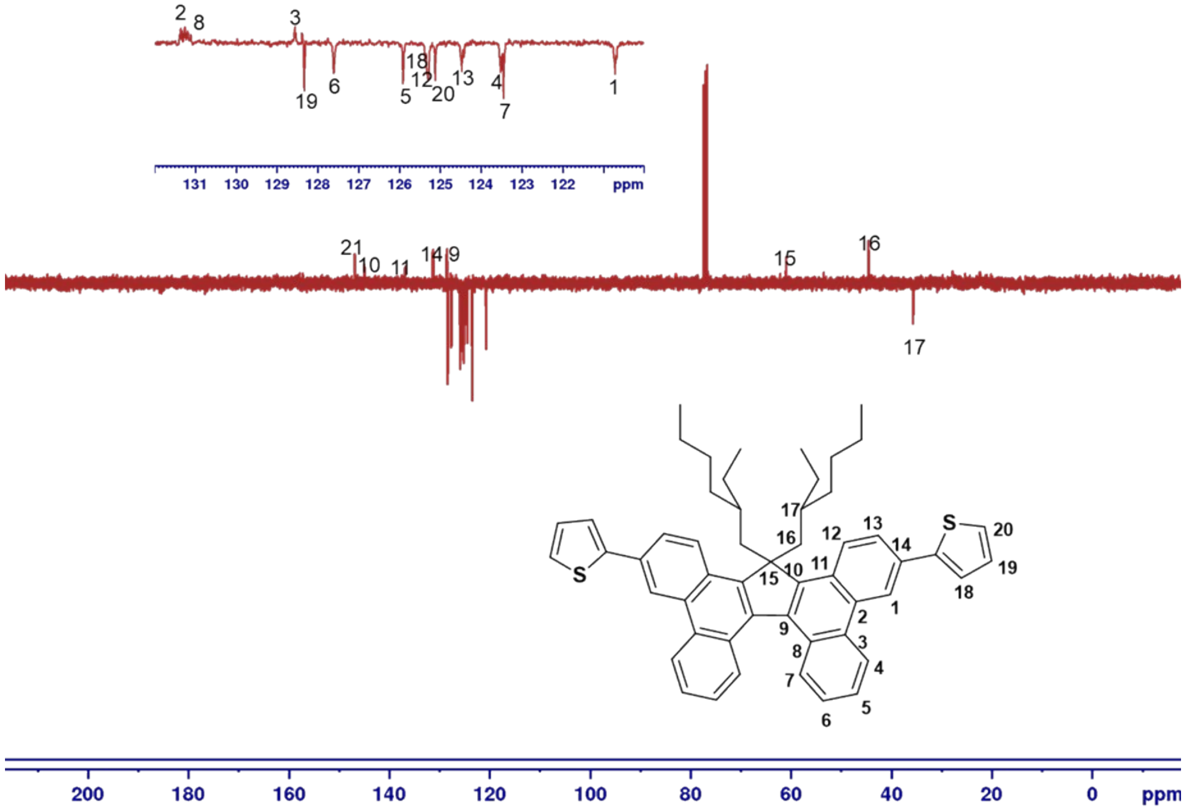

Figure S15. JMOD of TBFT2 in $CDCl_3$ at 298 K.

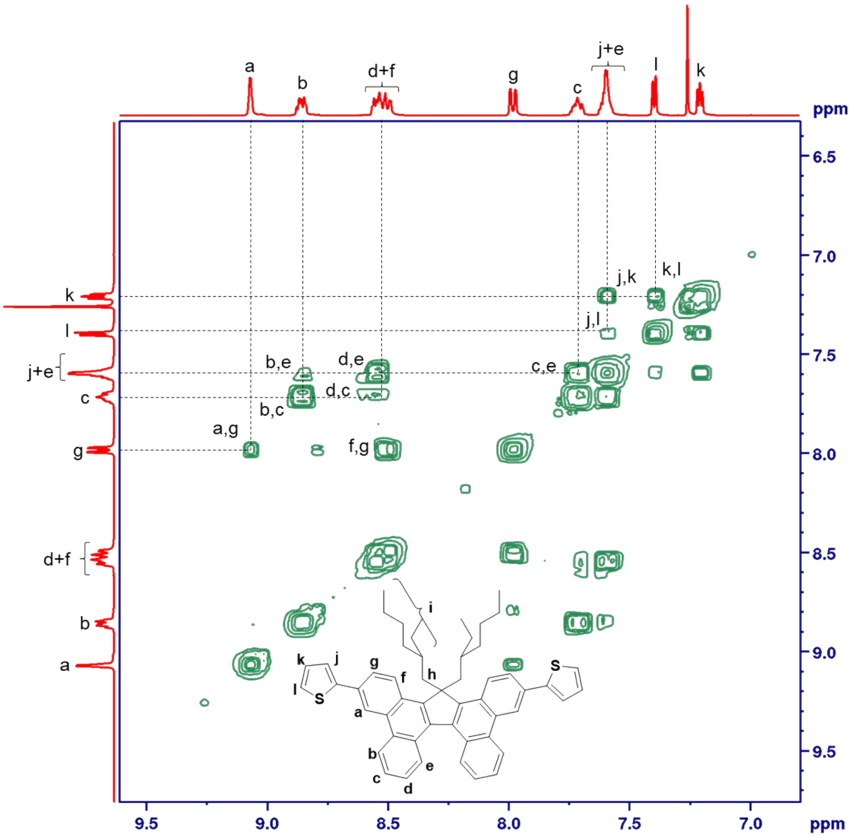

Figure S16: ^1H-^1H COSY spectrum of TBFT2 in $CDCl_3$ at 298 K.

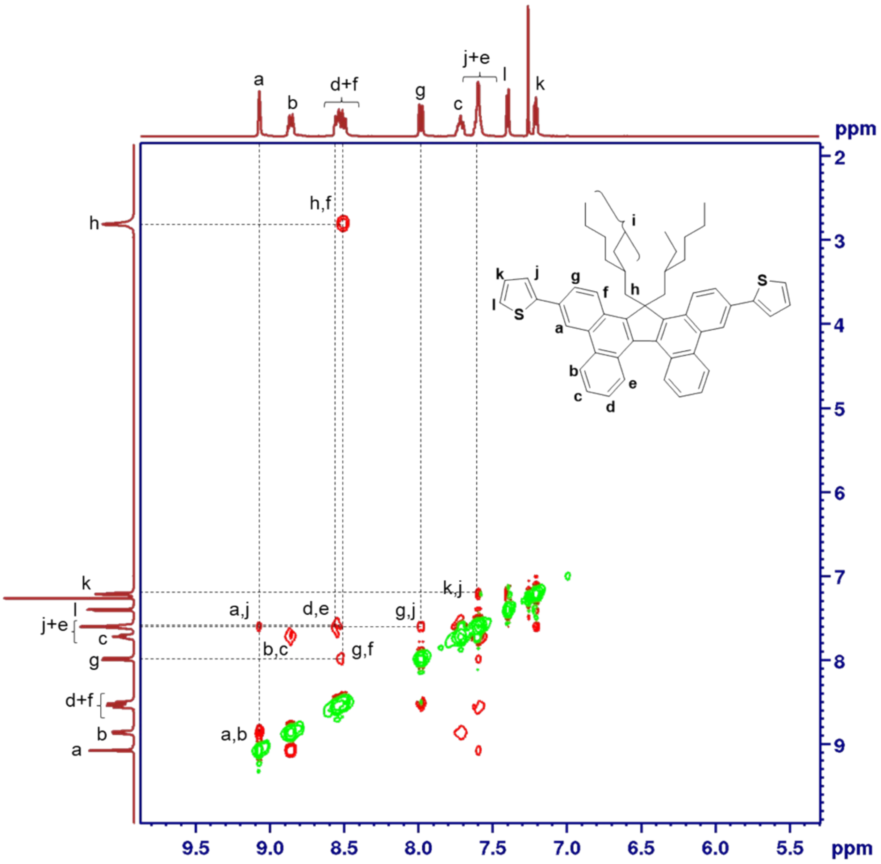

Figure S17: ^{1}H-^{1}H NOESY spectrum of TBFT2 in CDCl$_3$ at 298 K.

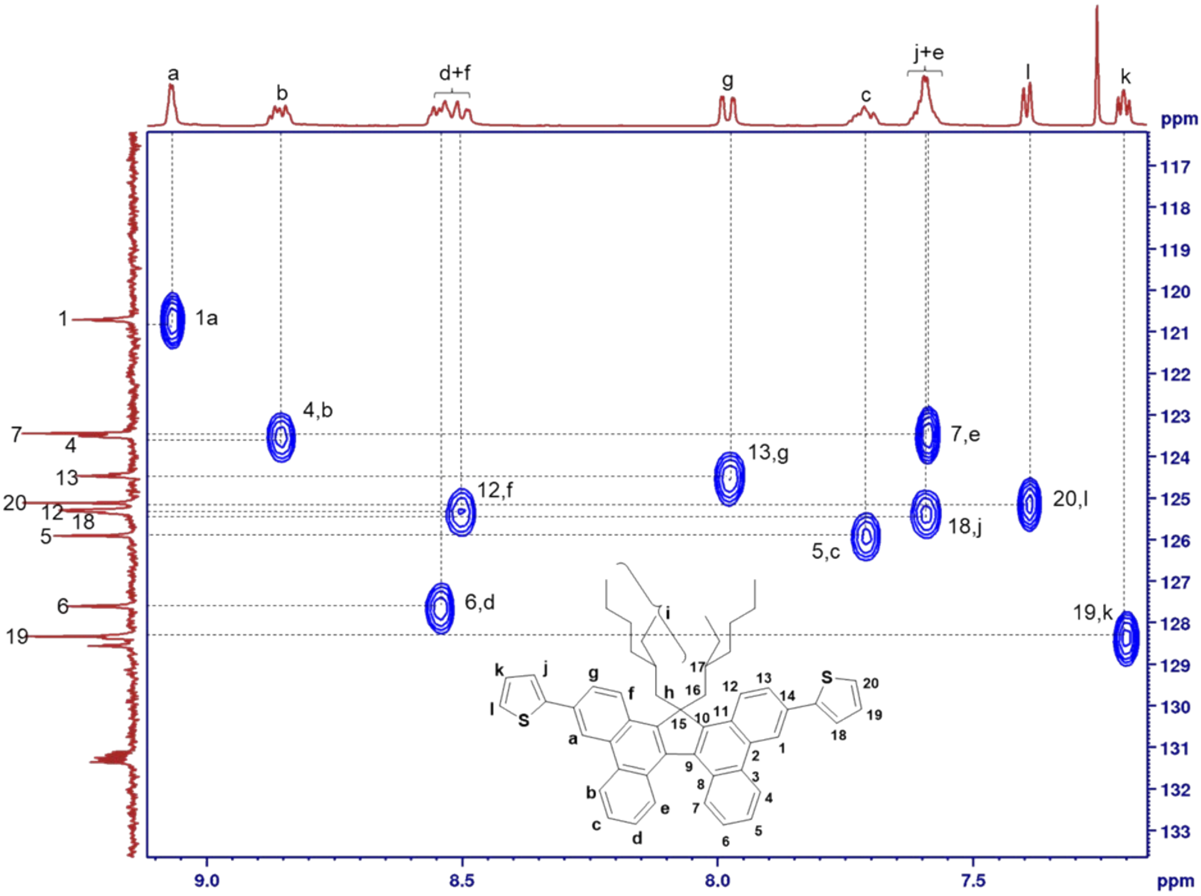

Figure S18: ^{1}H-^{13}C HSQC spectrum of TBFT2 in CDCl$_3$ at 298 K.

Section E. NMR studies of TBFT3

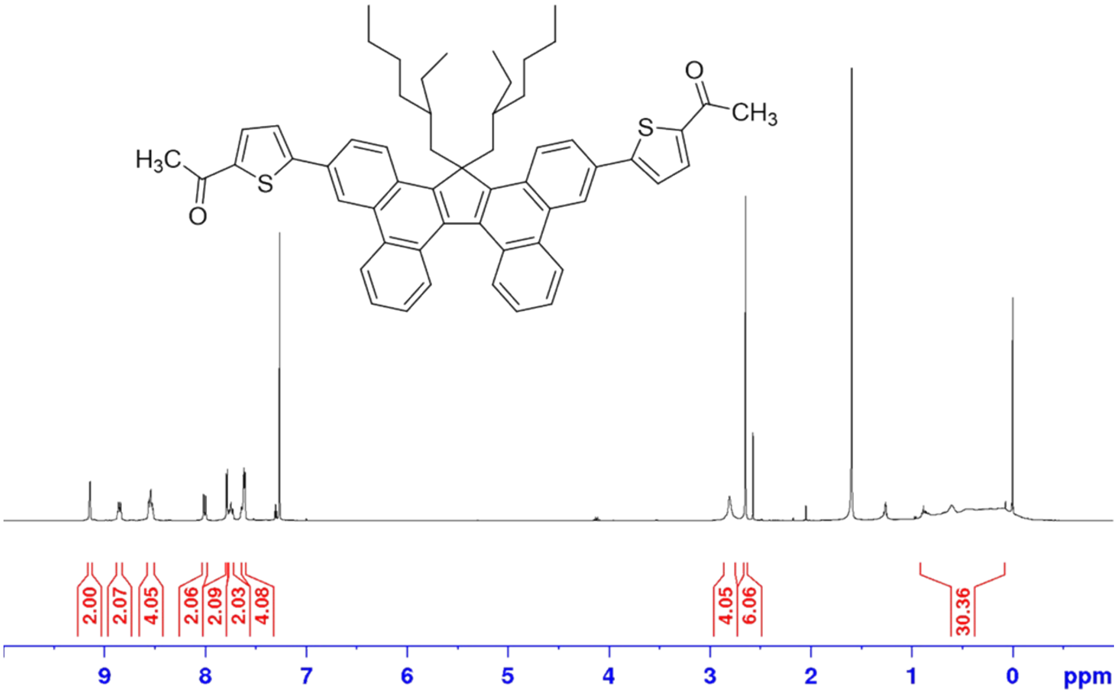

Figure S19. ^{1}H NMR spectrum of TBFT3 in CDCl$_3$ at 298 K.

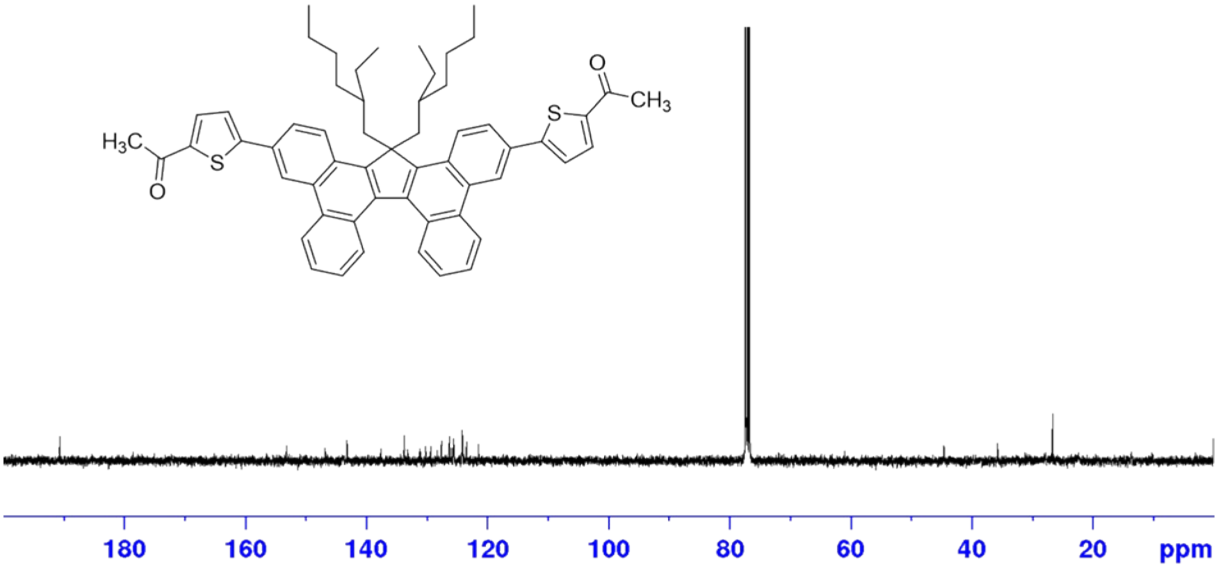

Figure S20. ^{13}C NMR spectrum of TBFT3 in CDCl$_3$ at 298 K.

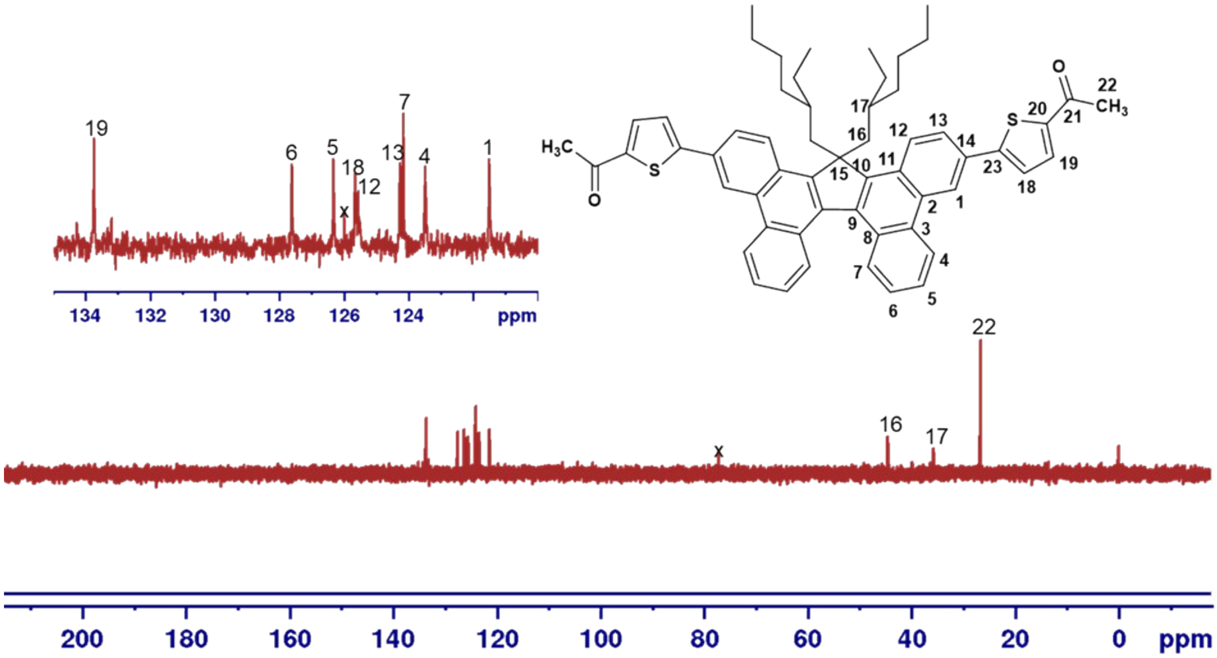

Figure S21. DEPT 45 of TBFT3 in CDCl$_3$ at 298 K.

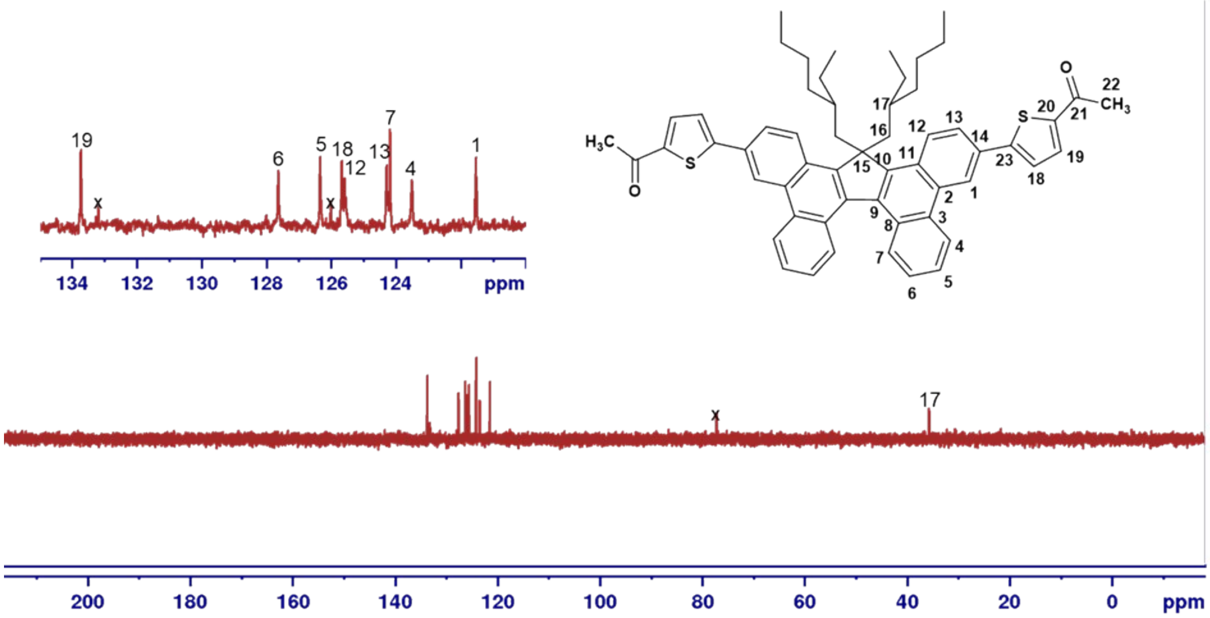

Figure S22. DEPT 90 of TBFT3 in CDCl$_3$ at 298 K.

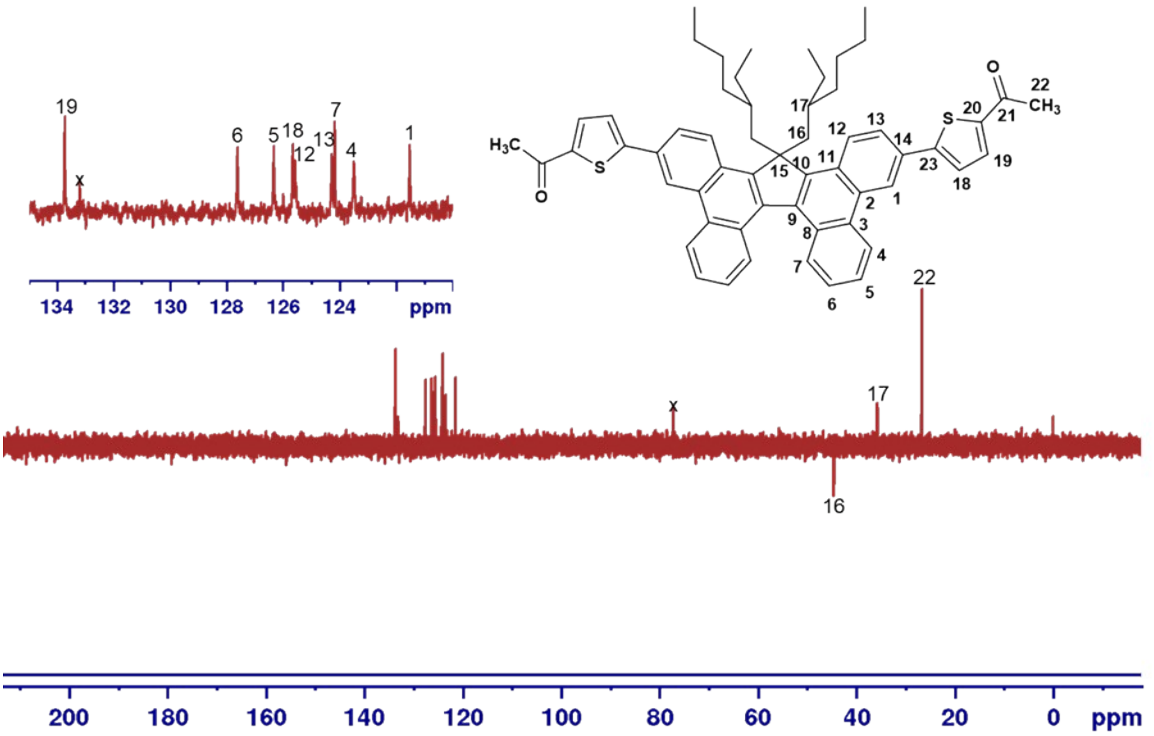

Figure S23. DEPT 145 of TBFT3 in $CDCl_3$ at 298 K.

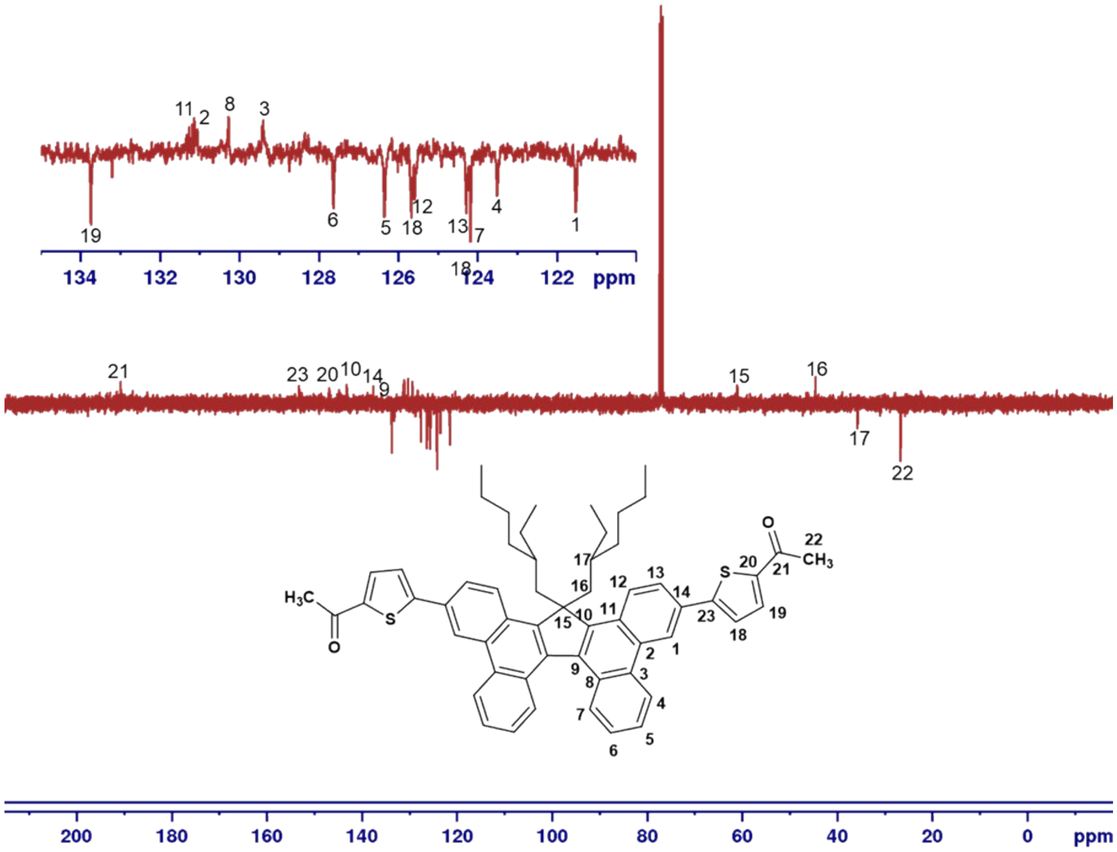

Figure S24. JMOD of TBFT3 in $CDCl_3$ at 298 K.

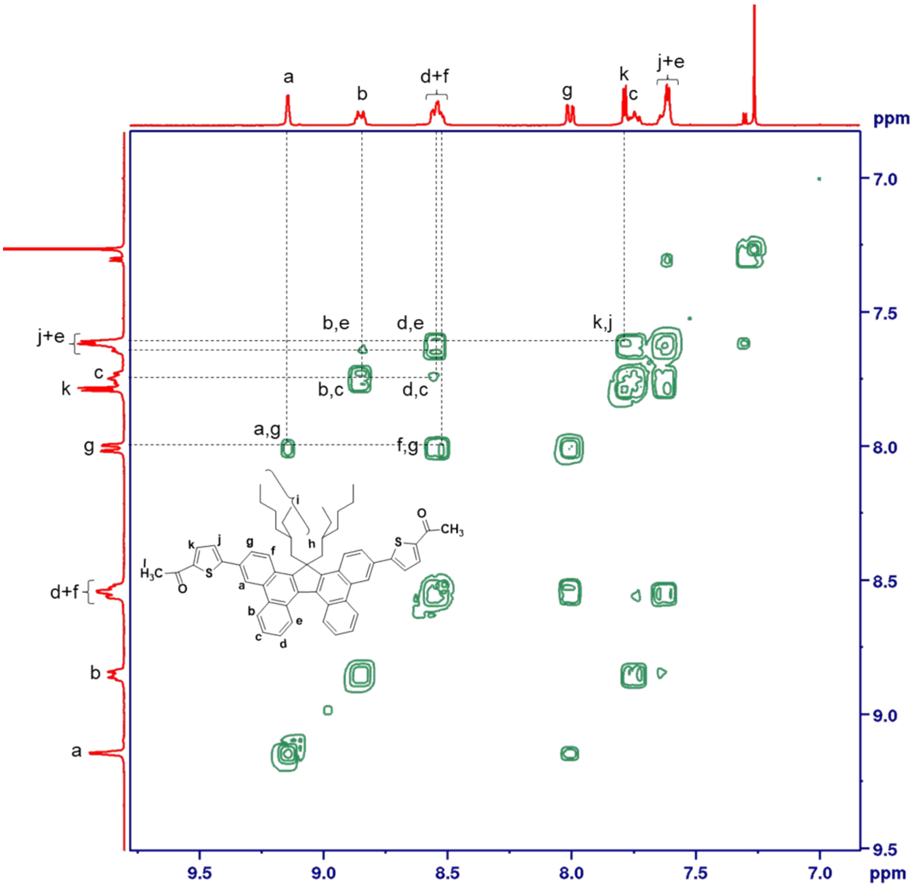

Figure S25. ^{1}H-^{1}H COSY spectrum of TBFT3 in CDCl$_3$ at 298 K.

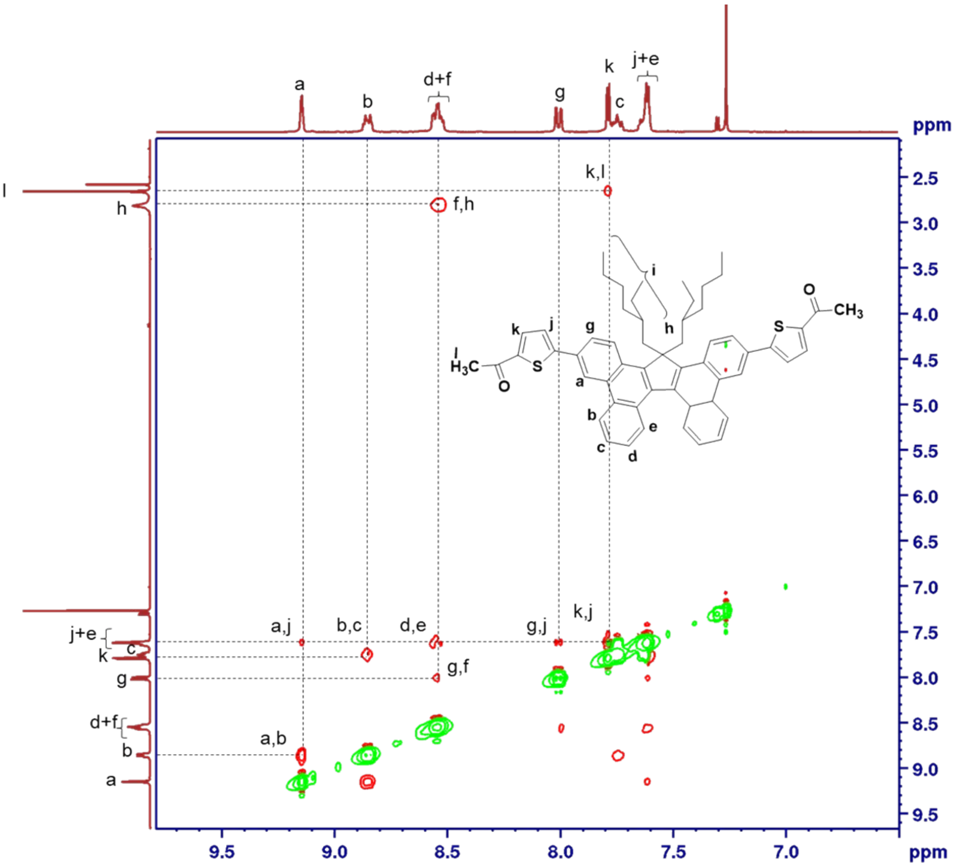

Figure S26. ^{1}H-^{1}H NOESY spectrum of TBFT3 in CDCl$_3$ at 298 K.

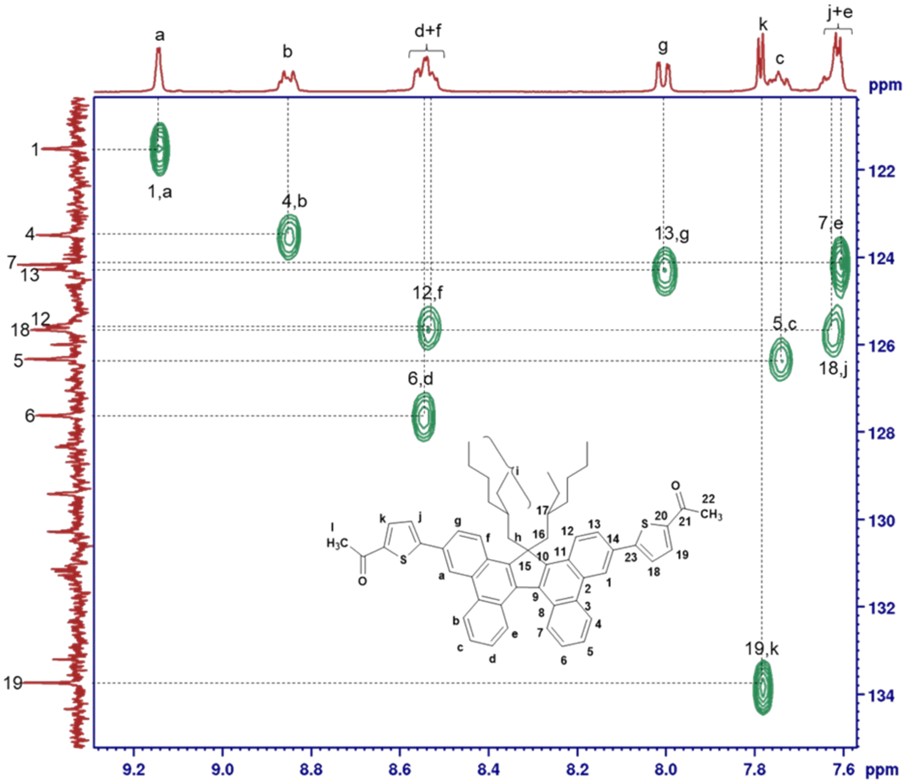

Figure S27. ^{1}H-^{13}C HSQC spectrum of TBFT3 in $CDCl_3$ at 298 K.

Section F. Thermogravimetric Analysis (TGA) Spectra of TBFT1-3

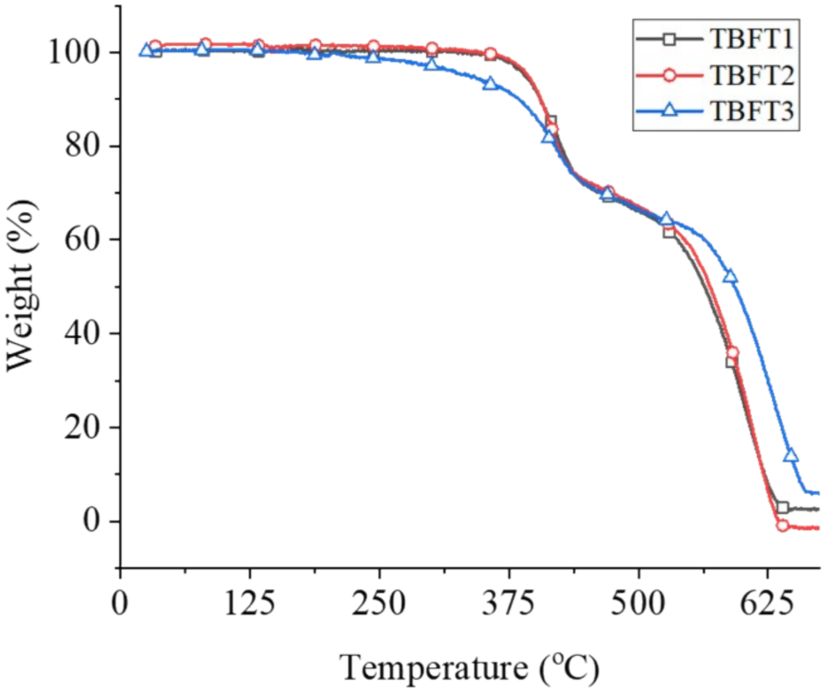

Figure S28. Thermogravimetric analysis (TGA) of TBFT1-3.

Section G. ATR-FTIR Spectra of TBFT1-3

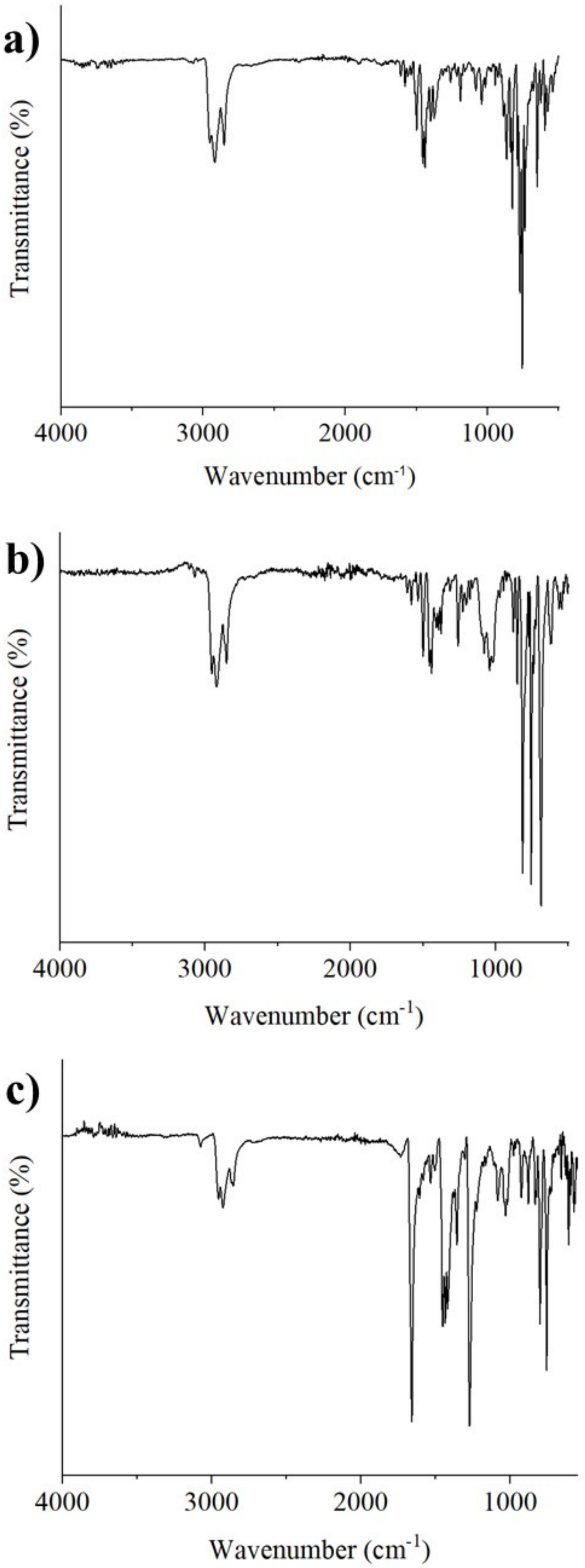

Figure S29. ATR- FTIR spectra of a) TBFT1, b) TBFT2, and c) TBFT3.

Section H. Optimized Geometries of TBFT1-3

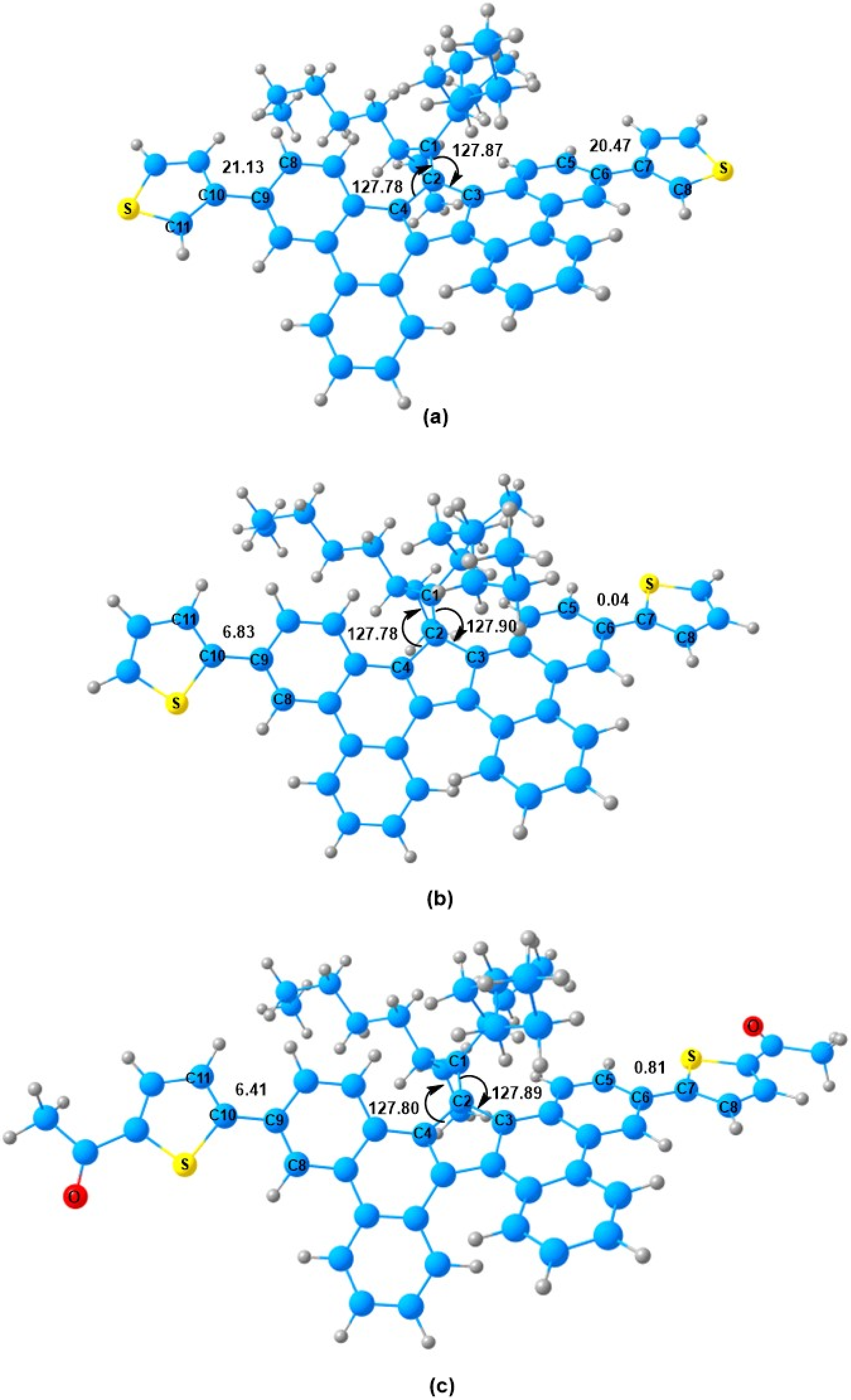

Figure S30. Optimized geometries of a) TBFT1, b) TBFT2, and c) TBFT3, Where the carbon, oxygen, sulfur, and hydrogen atoms are given in blue, red, yellow, and grey color, respectively. Dihedral angles are mentioned in degrees (º).

Section I. Electrochemical Studies of TBFT1-3

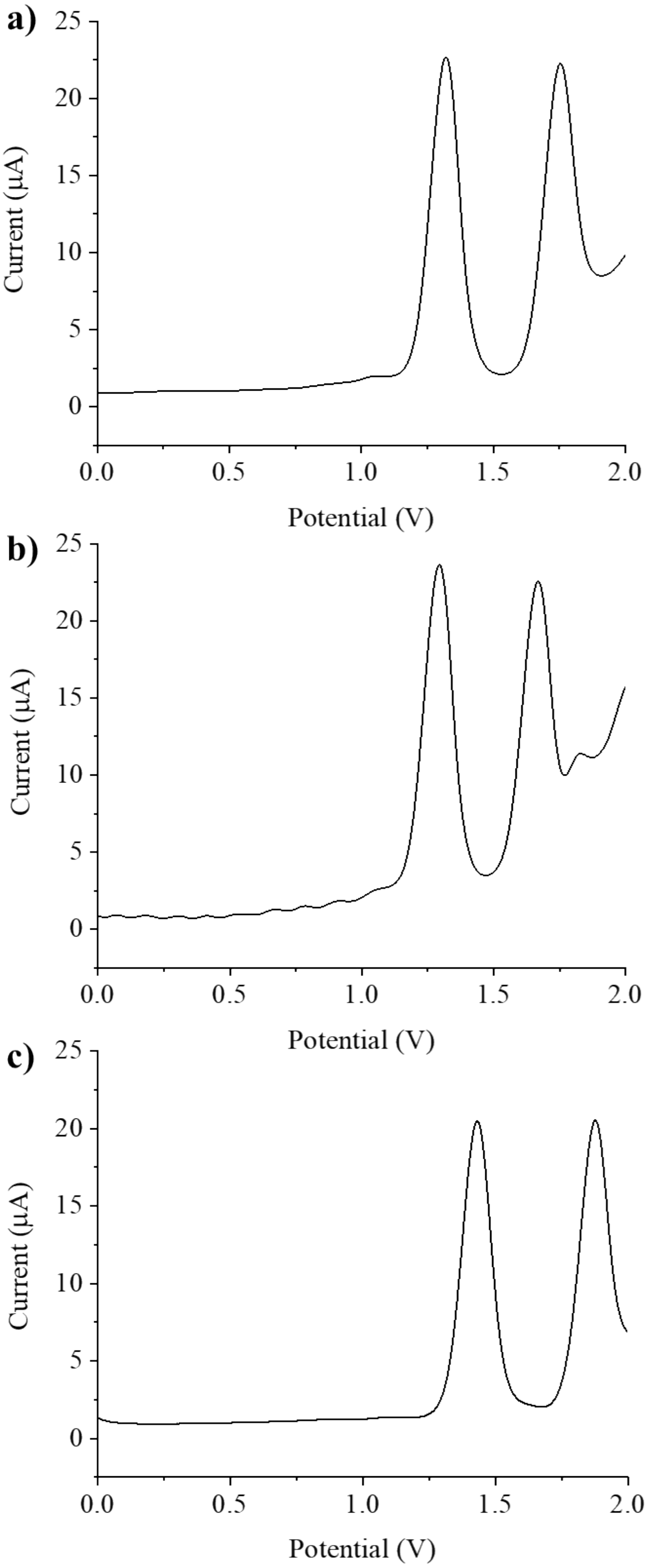

Figure S31. Differential Pulse Voltammogram of a) TBFT1, b) TBFT2, and c) TBFT3 in DCM (1×10^{-3} M) with $TBAPF_6$ (0.1 M) as the supporting electrolyte, glassy carbon electrode as working electrode, Pt wire as the counter electrode and calomel electrode as the reference electrode.

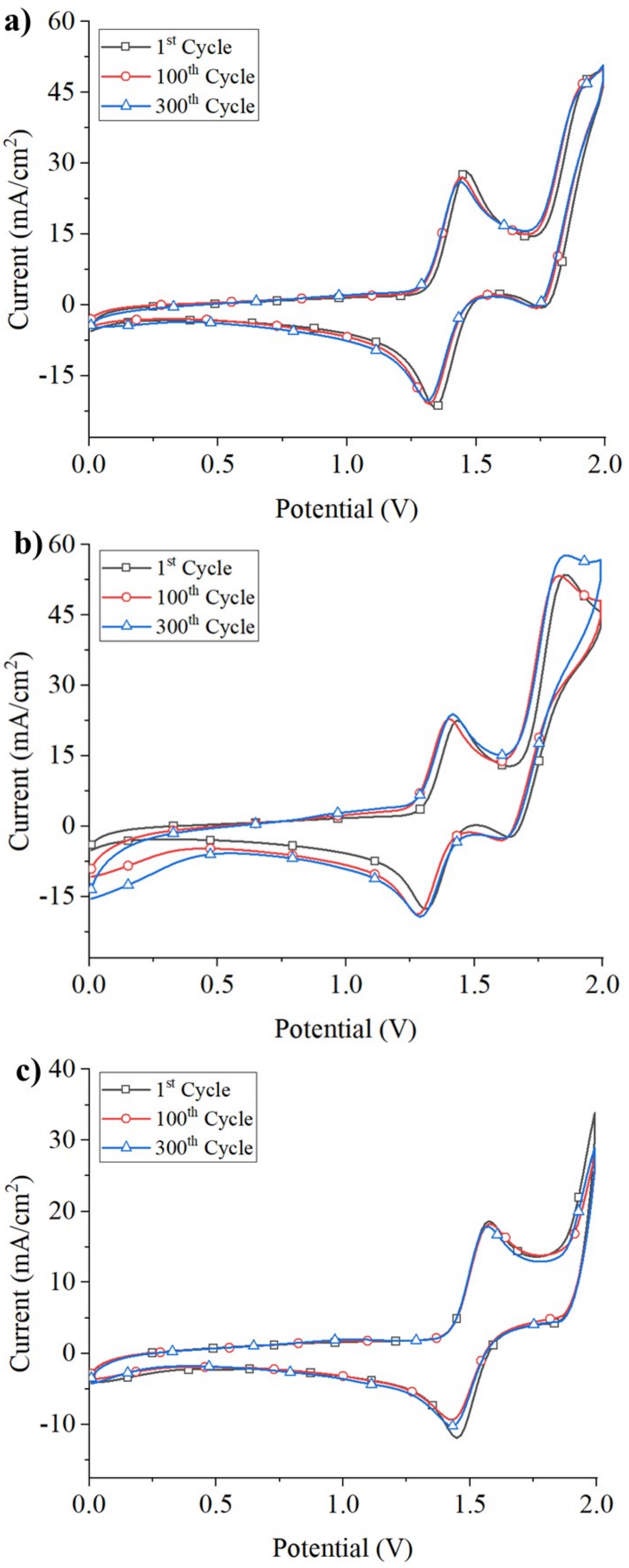

Figure S32. Cyclic Voltammogram of a) TBFT1, b) TBFT2, and c) TBFT3 with continuous scan for 300 cycles at a scan rate of 100 mV/s in DCM (1×10^{-3} M) with TBAPF$_6$ (0.1 M) as the supporting electrolyte, glassy carbon electrode as working electrode, Pt wire as the counter electrode and calomel electrode as the reference electrode.

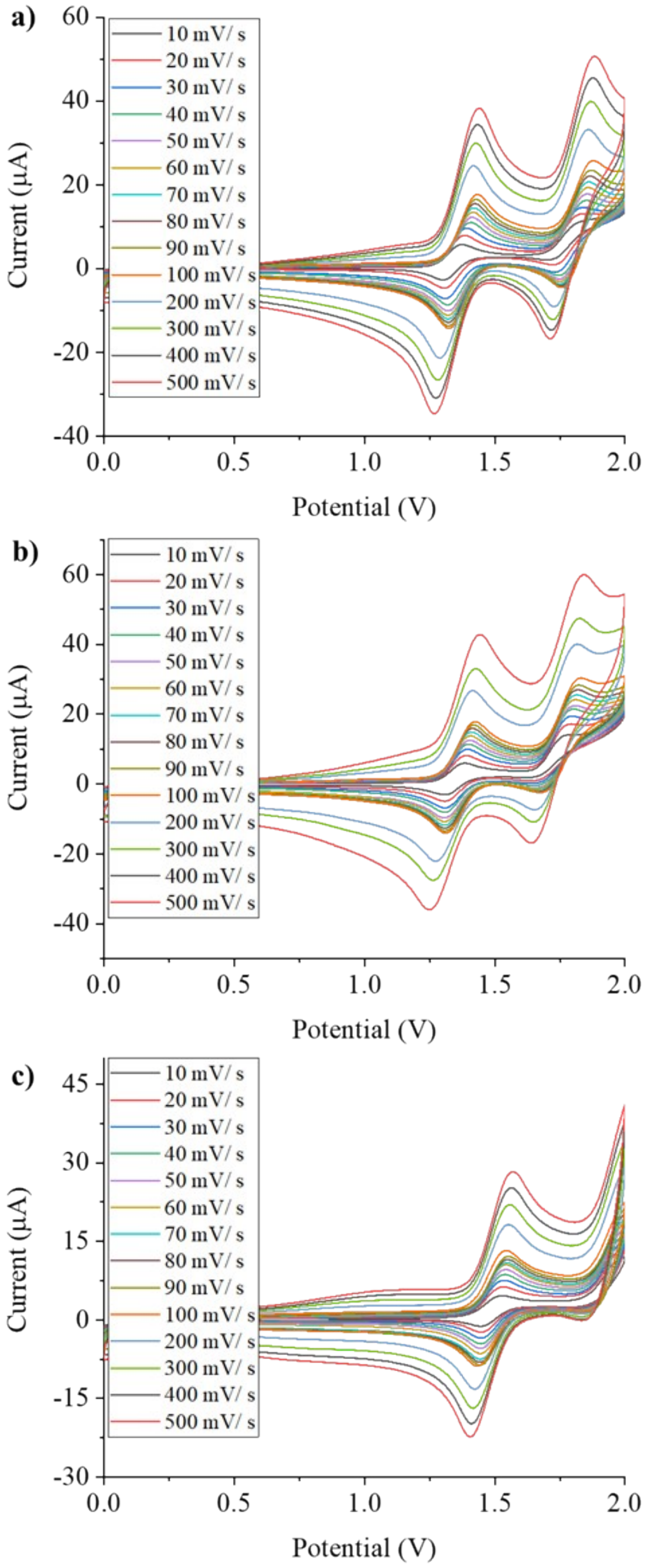

Figure S33. Cyclic Voltammogram at different scan rates of a) TBFT1, b) TBFT2, and c) TBFT3 in DCM (1 × 10^{-3} M) with $TBAPF_6$ (0.1 M) as the supporting electrolyte, glassy carbon electrode as working electrode, Pt wire as the counter electrode and calomel electrode as the reference electrode.

Section J. Spectroelectrochemistry Studies of TBFT1-3

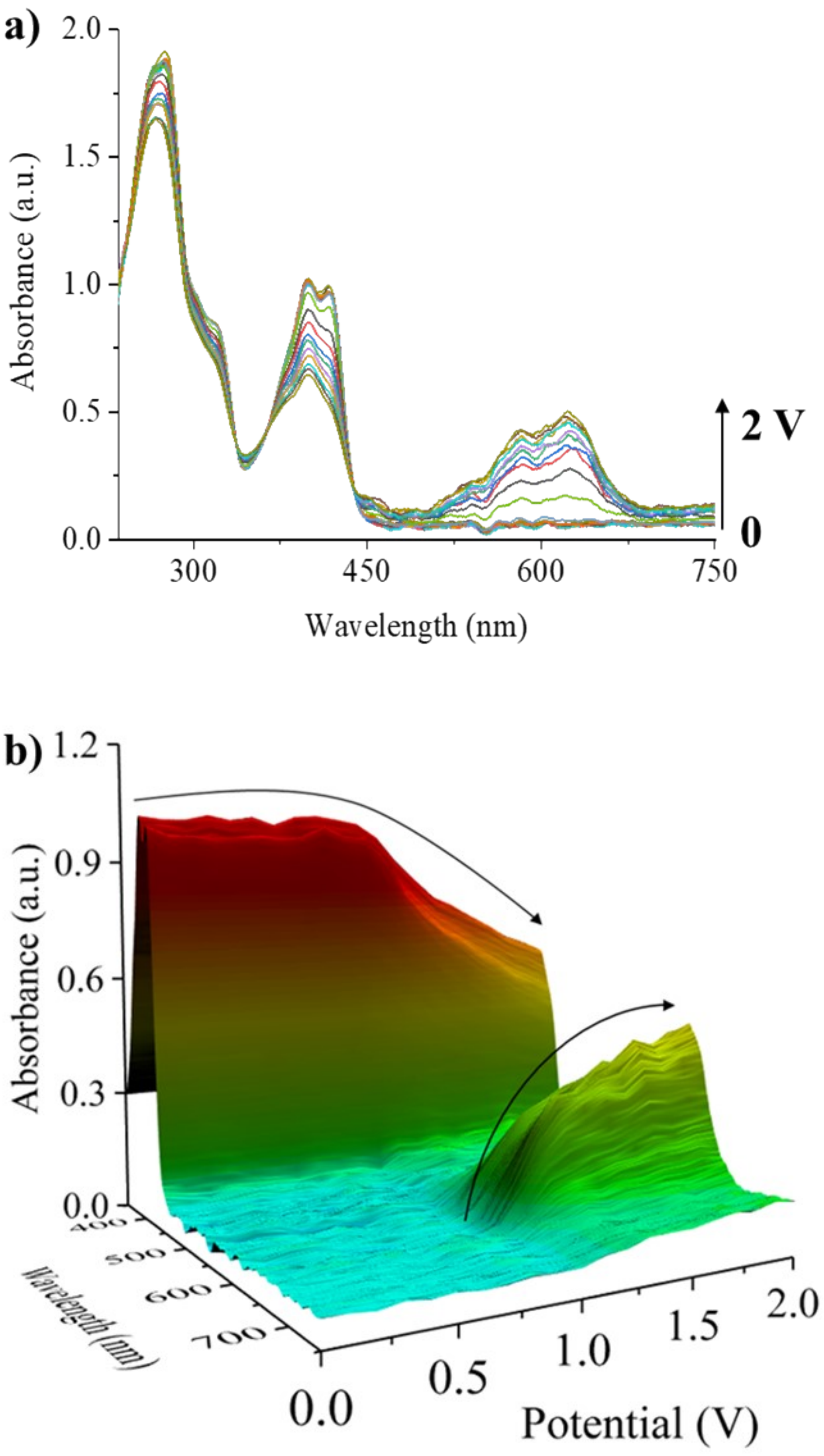

Figure S34. Spectroelectrochemistry of TBFT1 a) 1D and b) 3D in DCM (1×10^{-3} M) with $TBAPF_6$ (0.1 M) as the supporting electrolyte, at applied potentials (0-2 V) carried out with Pt mesh working electrode, Pt wire counter electrode and Ag/Ag^+ quasi reference electrode.

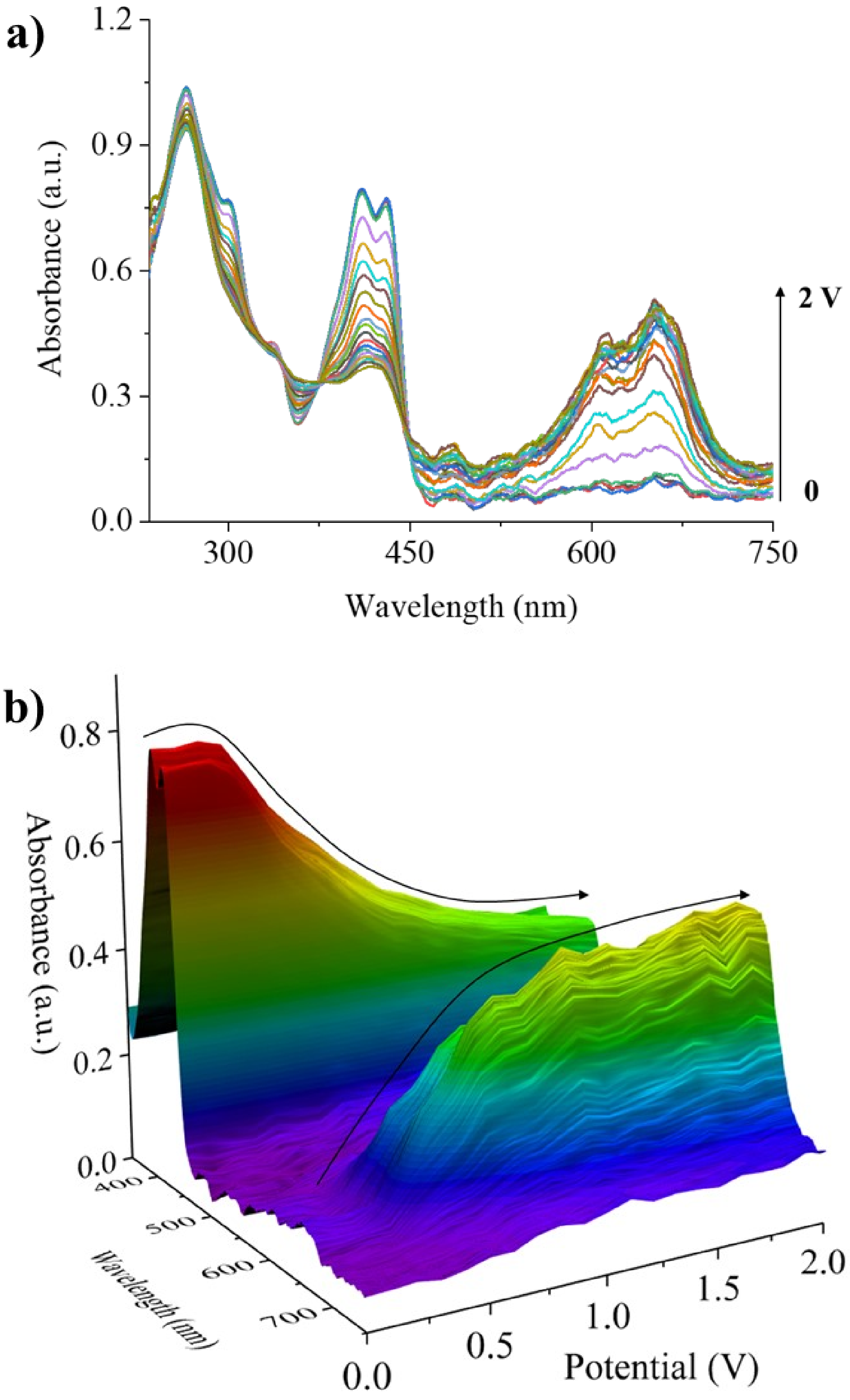

Figure S35. Spectroelectrochemistry of TBFT2 a) 1D and b) 3D in DCM (1×10^{-3} M) with $TBAPF_6$ (0.1 M) as the supporting electrolyte at applied potentials (0-2 V) carried out with Pt mesh working electrode, Pt wire counter electrode, and Ag/Ag^+ quasi reference electrode.

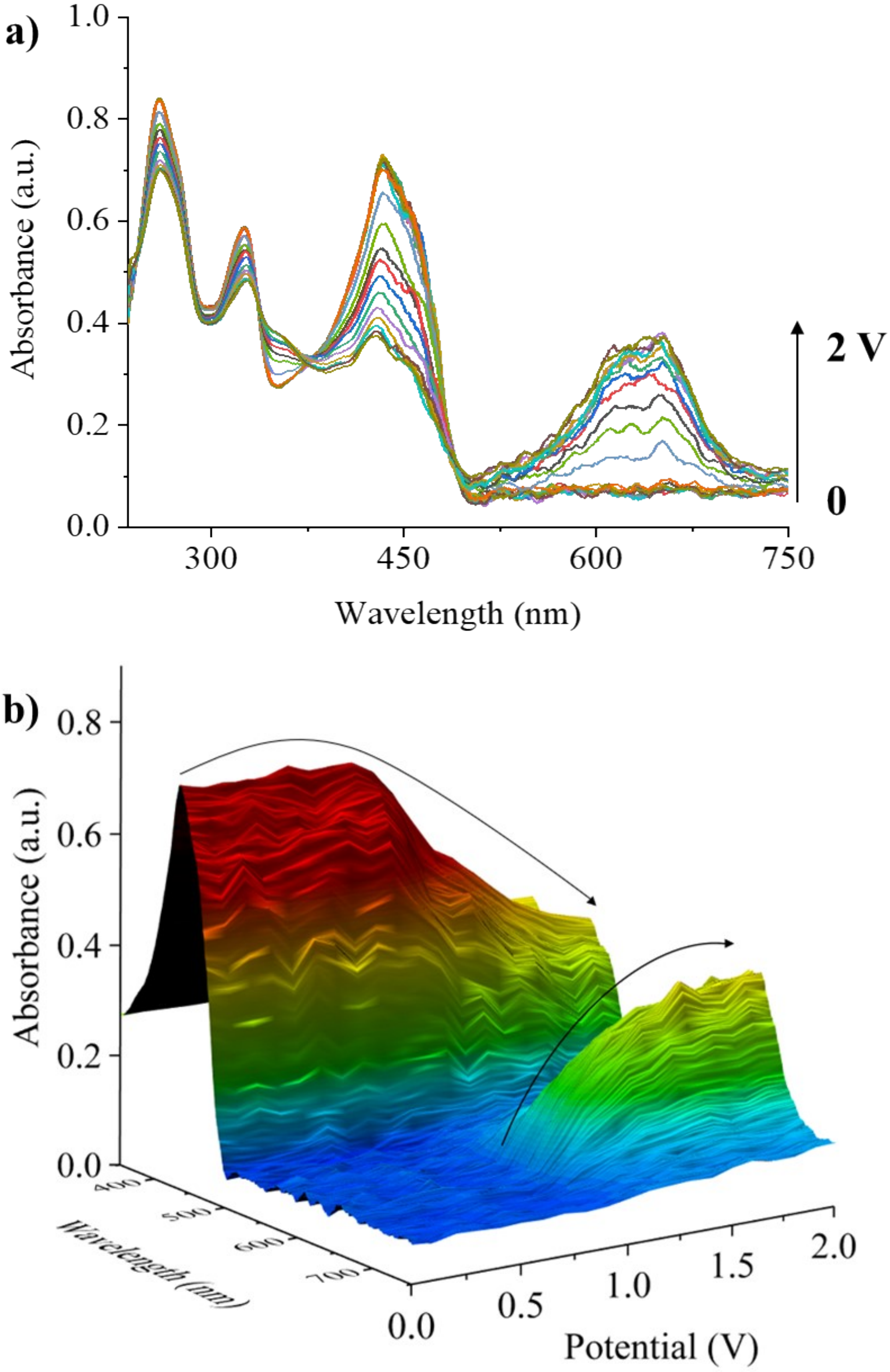

Figure S36. Spectroelectrochemistry of TBFT3 a) 1D and b) 3D in DCM (1 × 10^{-3} M) with $TBAPF_6$ (0.1 M) as the supporting electrolyte at applied potentials (0-2 V) carried out with Pt mesh working electrode, Pt wire counter electrode and Ag/Ag^+ quasi reference electrode.

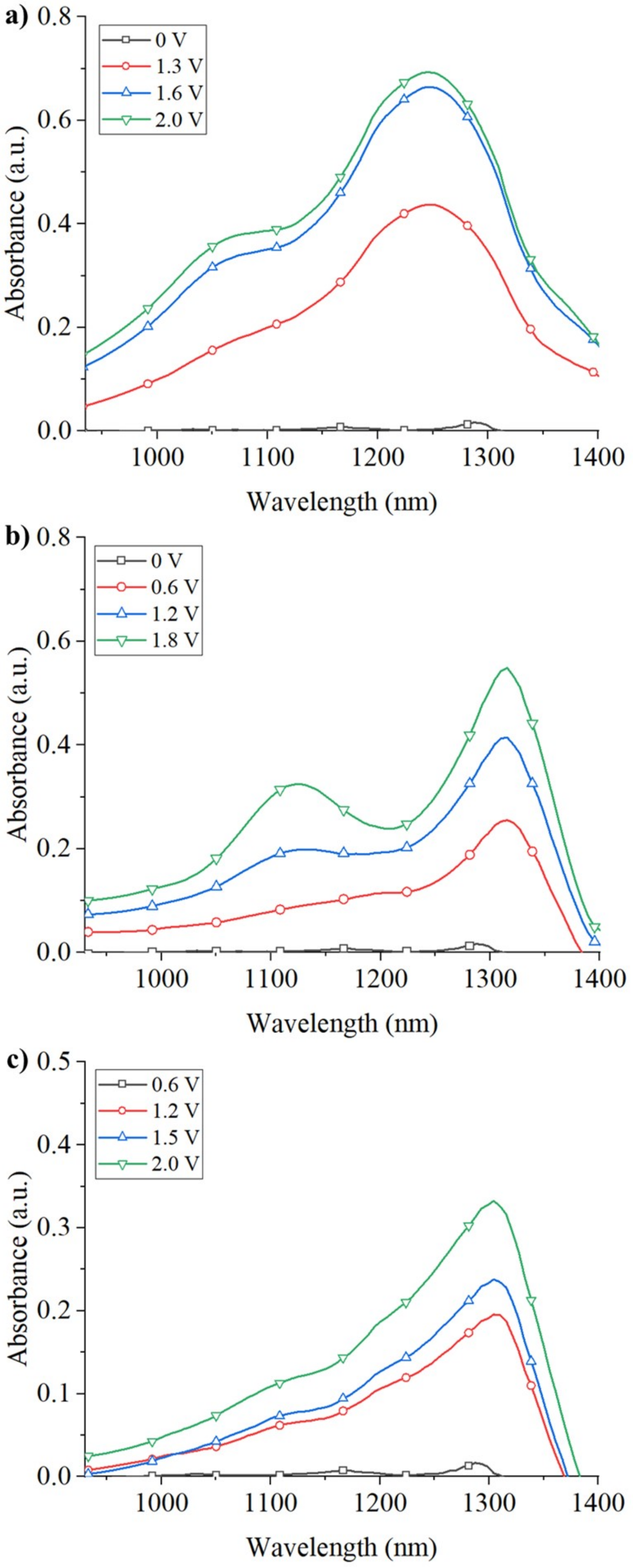

Figure S37. The NIR spectra of a) TBFT1, b) TBFT2 and c) TBFT3 in DCM (1×10^{-3} M) with $TBAPF_6$ (0.1 M) as the supporting electrolyte at applied potentials (0-2 V) carried out with Pt mesh working electrode, Pt wire counter electrode and Ag/Ag^+ quasi reference electrode.

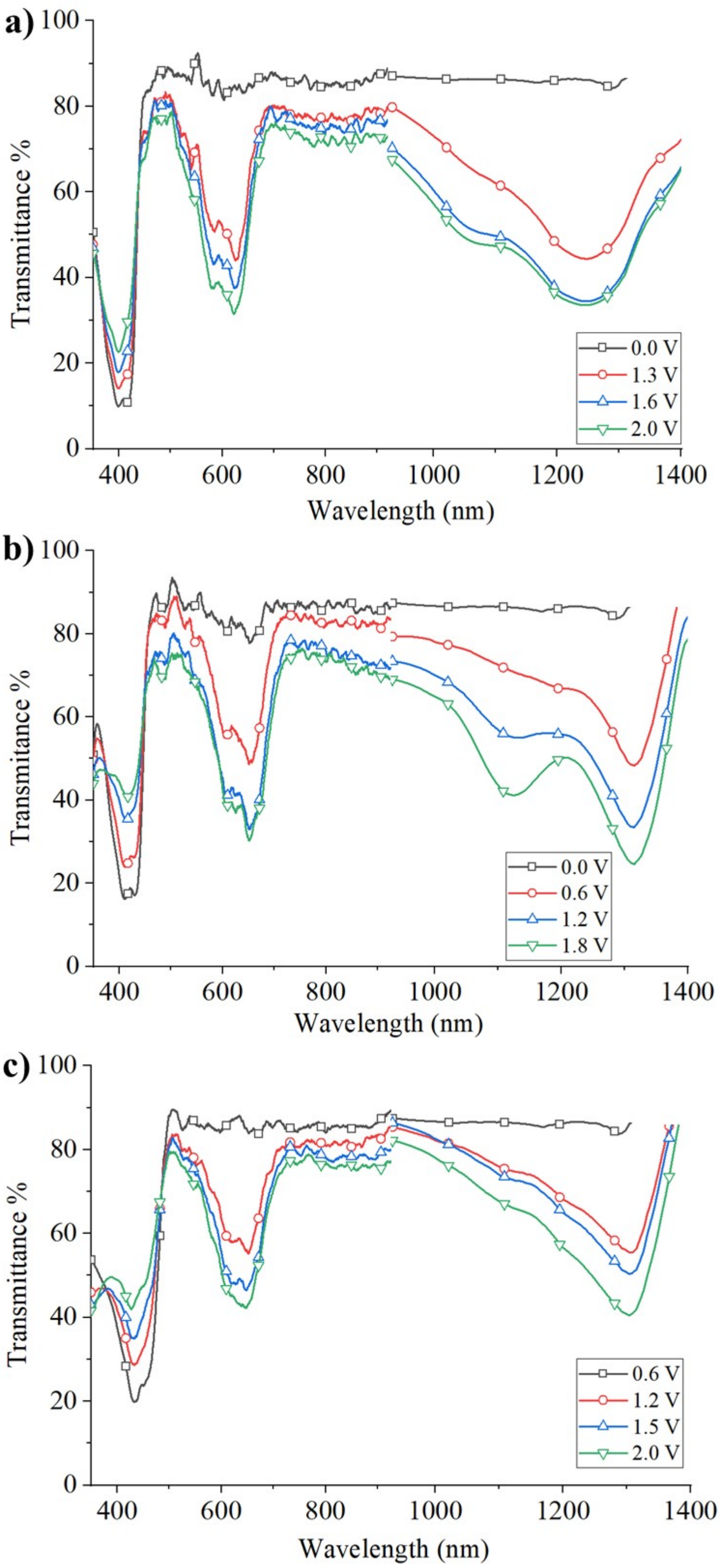

Figure S38. The spectroelectrochemistry plots of a) TBFT1, b) TBFT2 and TBFT3 in terms of transmittance vs. wavelength in DCM (1×10^{-3} M) with $TBAPF_6$ (0.1 M) as the supporting electrolyte at applied potentials (0-2 V) carried out with Pt mesh working electrode, Pt wire counter electrode and Ag/Ag^+ quasi reference electrode.

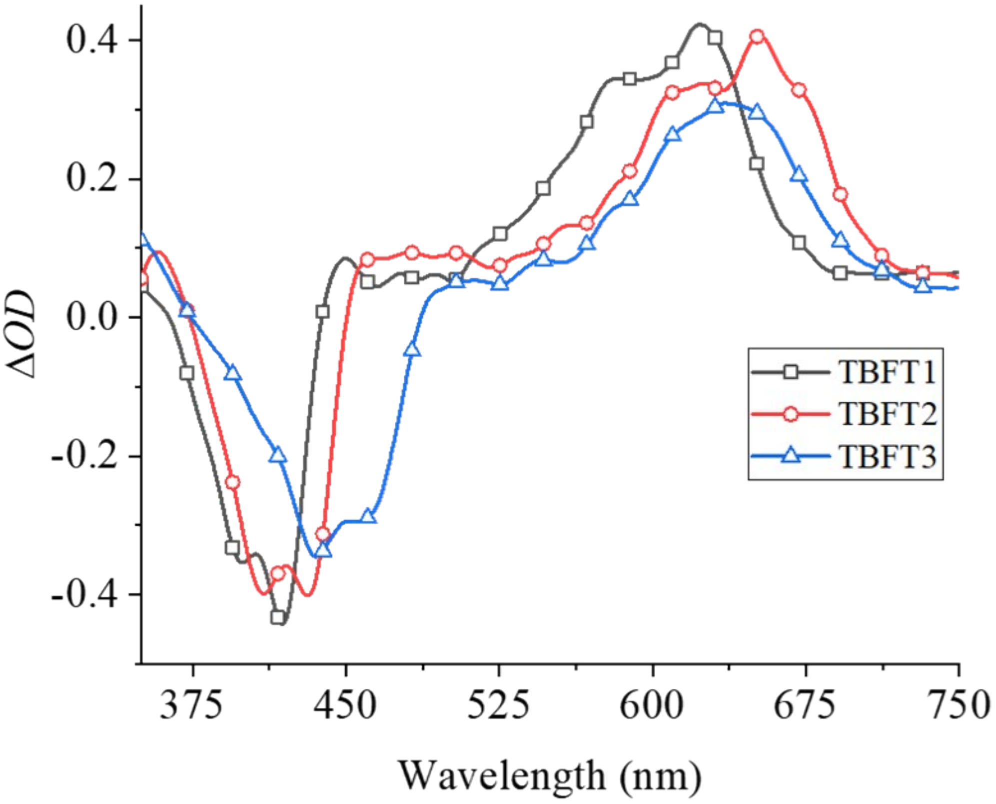

Figure S39. Optical density changes of the molecules at various wavelengths.

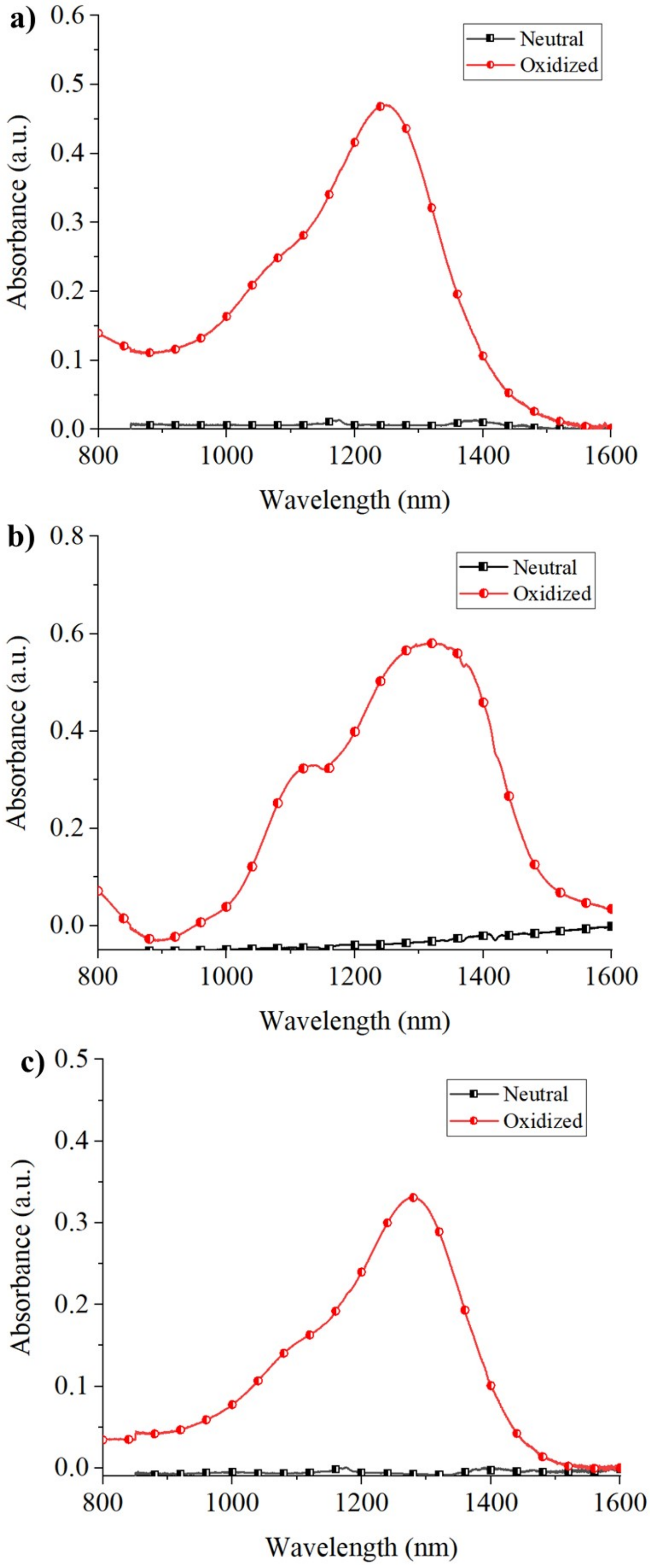

Figure S40. The modulation ability of solid-state device in the NIR region: a) TBFT1 and b) TBFT2 and c) TBFT3.

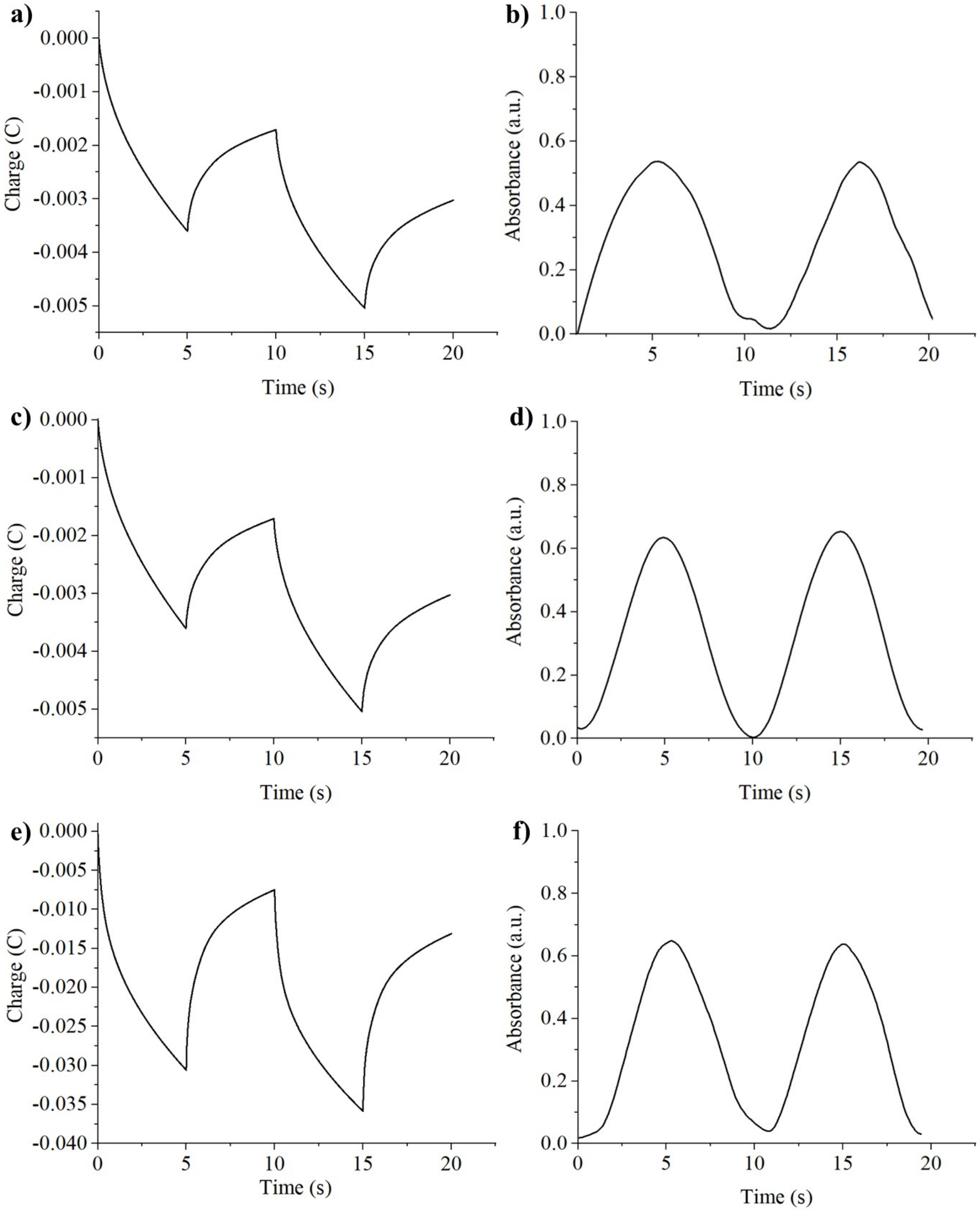

Figure S41. Chronocoulometric plots and absorbance changes of a & b) TBFT1, c & d) TBFT2 and e & f) TBFT3 respectively.

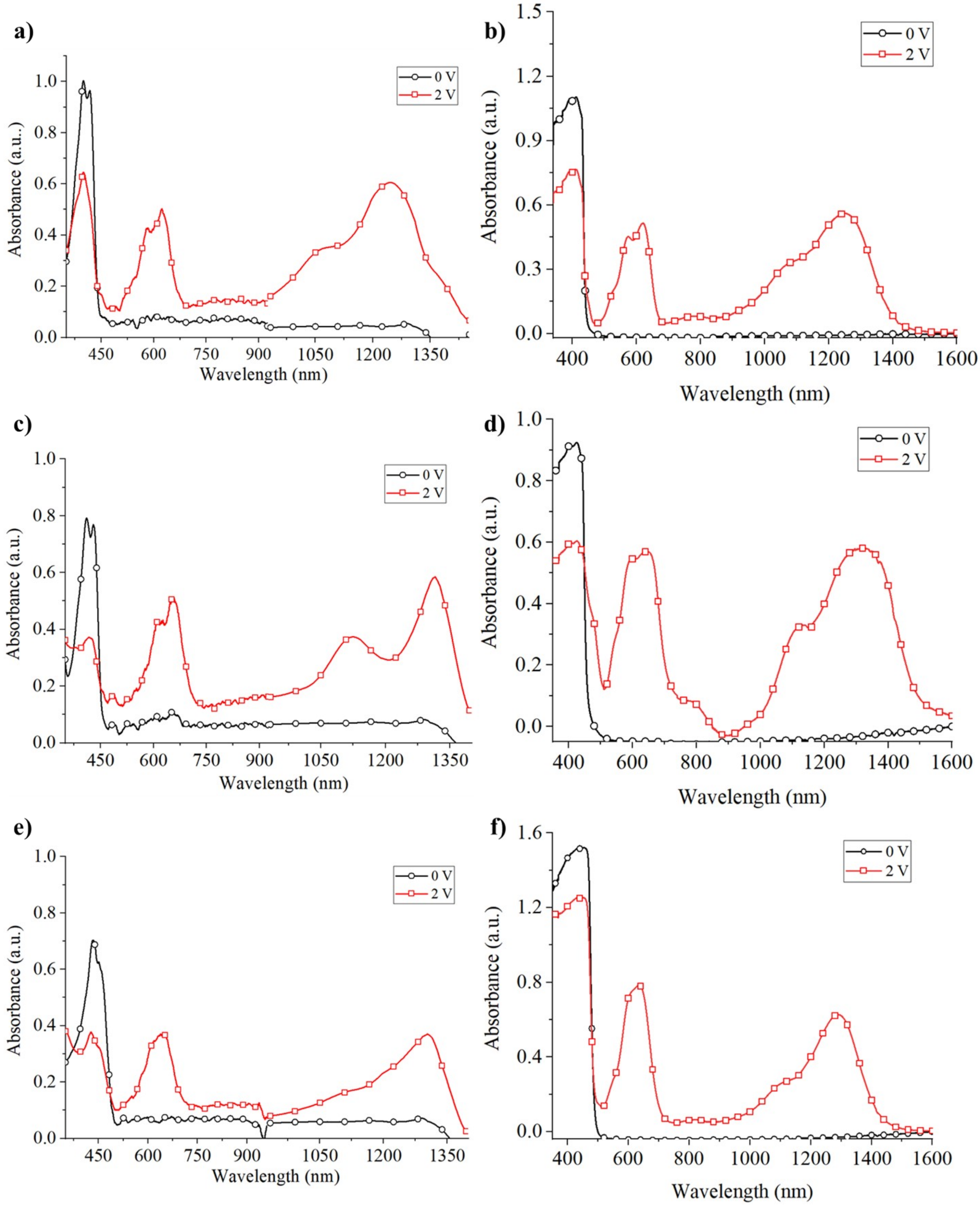

Figure S42. The spectroelectroscopy plots of a & b) TBFT1, c & d) TBFT2 and e & f) TBFT3 in DCM at two different concentrations: a, c & e) 1.5 x 10 $^{-5}$ M and b, d & f) 2 x 10 $^{-5}$ M.

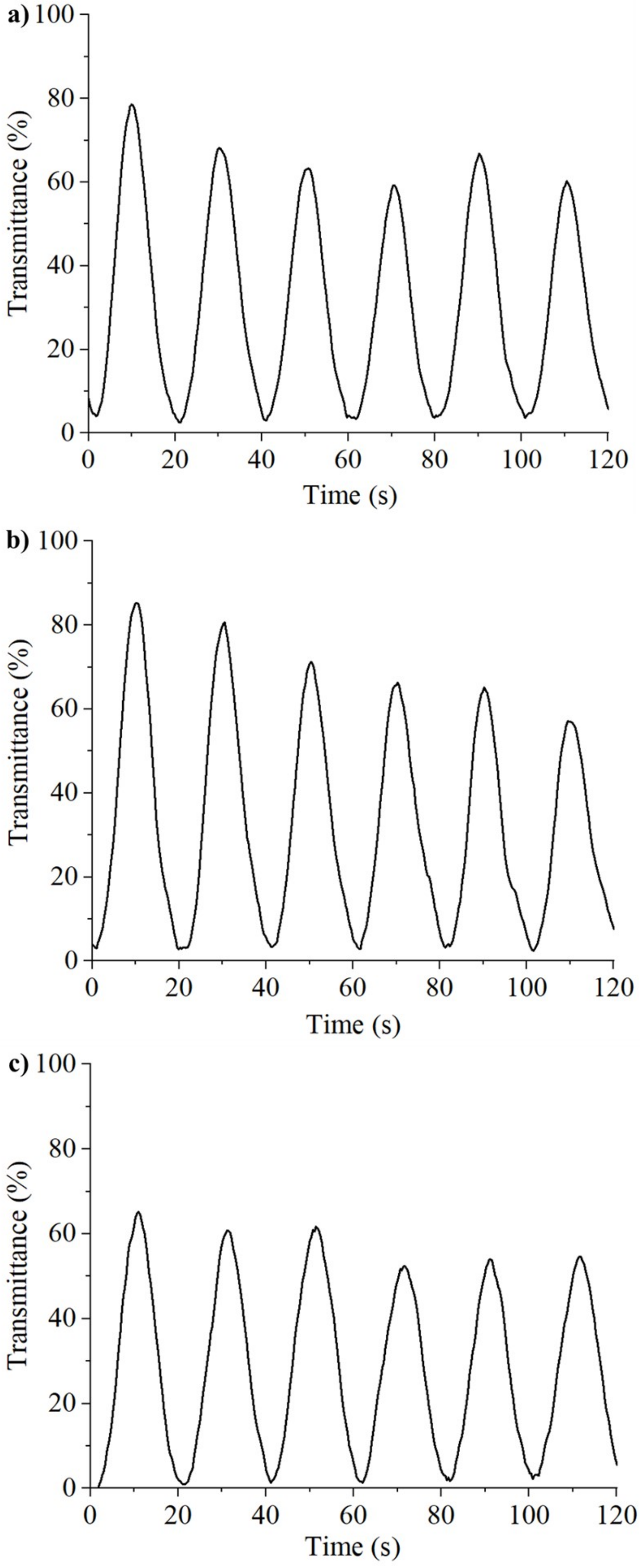

Figure S43. EC switching (potential switched between 0-2 V) of a) TBFT1, b) TBFT2, and c) TBFT3 at radical cation's wavelengths in 0.1 M $TBAPF_6$ in DCM measured using Pt mesh as working electrode, Pt wire is taken as counter electrode and Ag/Ag^+ as quasi reference electrode with a switching time of 10 s.

Section K. Colorimetry Studies of TBFT1-3

Table S1. *L*a*b** values and CIE coordinates of TBFT1-3.

Compound	Neutral					Colored				
	*L**	*a**	*b**	CIE		*L**	*a**	*b**	CIE	
				x	y				x	y
TBFT1	70	-1	4	0.32	0.34	47	-7	-45	0.18	0.20
TBFT2	68	-8	23	0.35	0.39	45	-28	-20	0.19	0.28
TBFT3	68	-14	68	0.42	0.50	41	-43	42	0.31	0.58

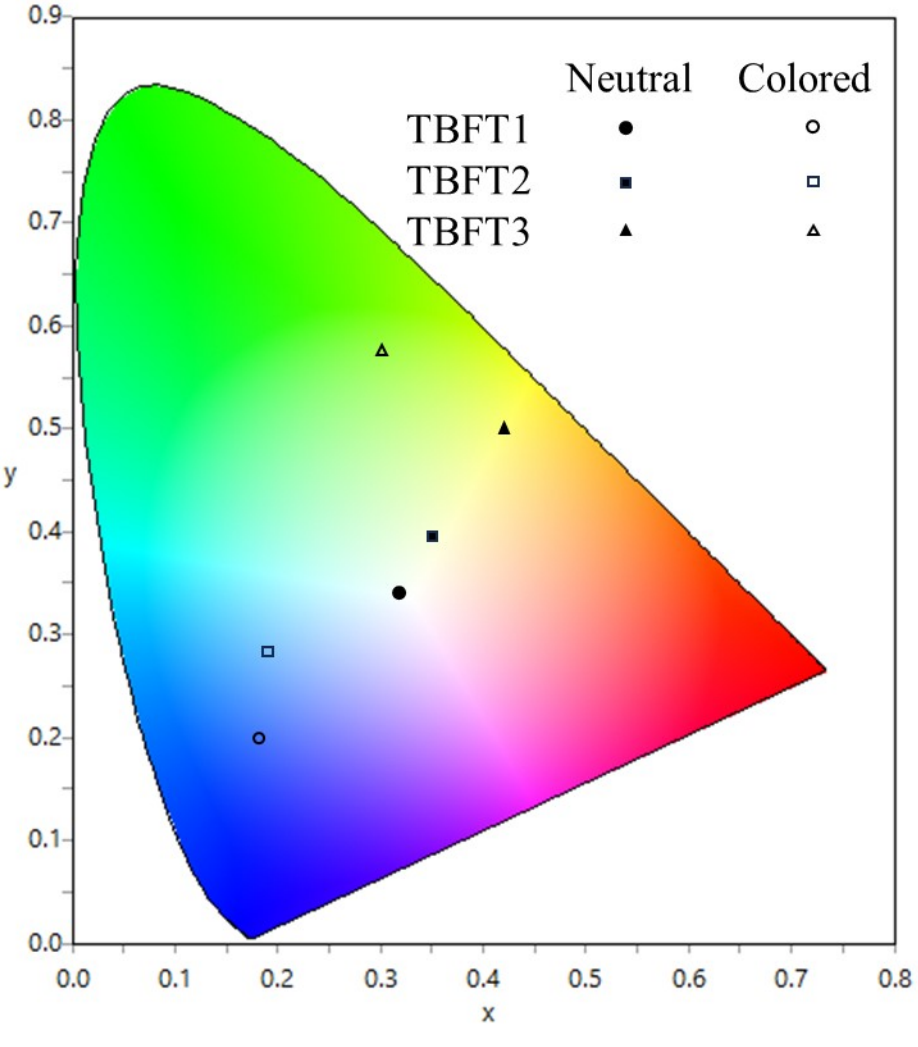

Figure S44. CIE chart of the compounds in the neutral and colored states.

Section L. Cyclic Voltammogram (CV) of Devices at different scan rates

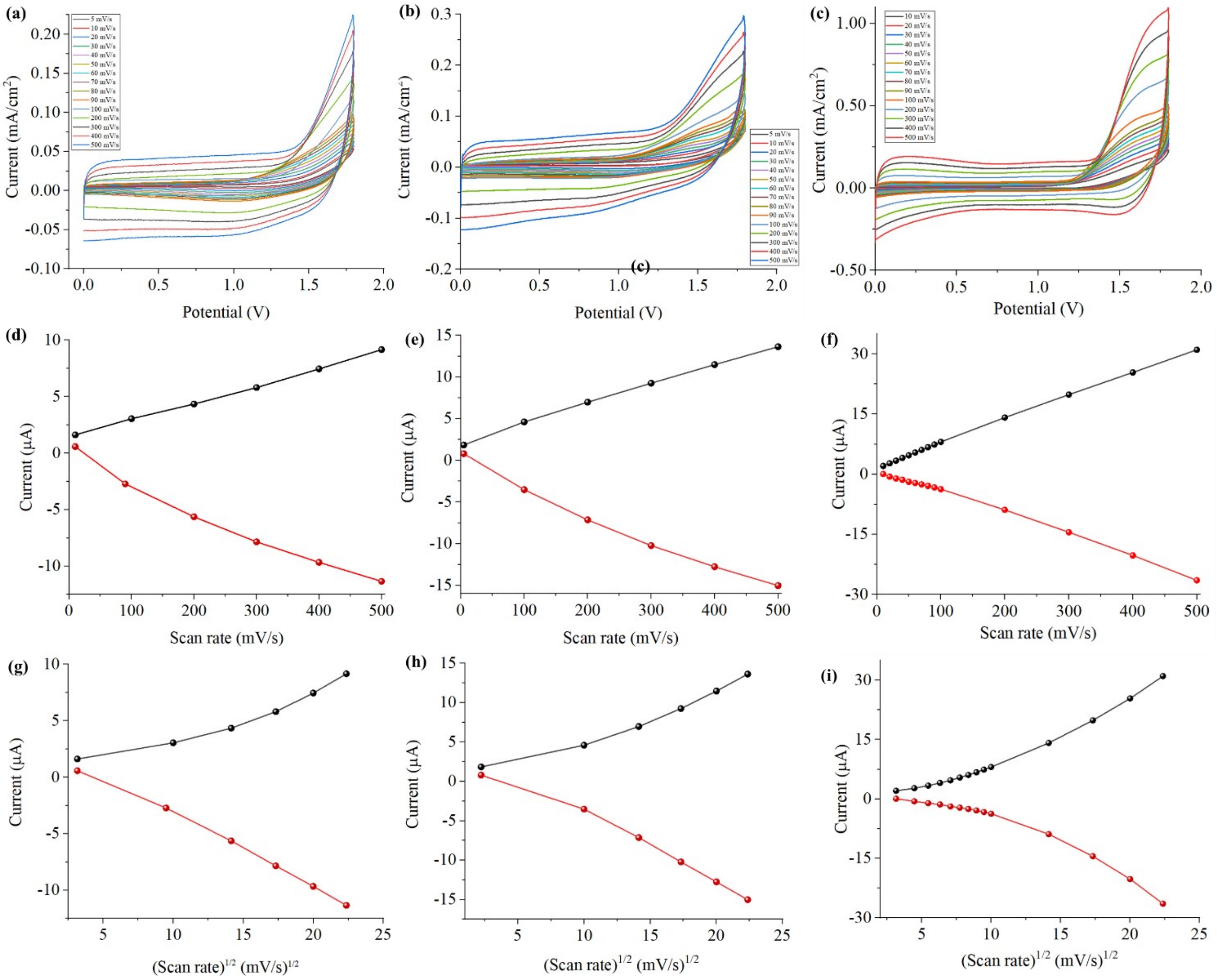

Figure S45. Cyclic Voltammogram of devices made of TBFT1 at different scan rates a) drop cast and b) drop cast with Nafion coating and c) gel sate. The dependence of current on the scan rates, d) drop cast, e) drop cast with nafion coating and f) gel; and the square root of the scan rates: g) drop cast, h) drop cast and nafion and i) gel.

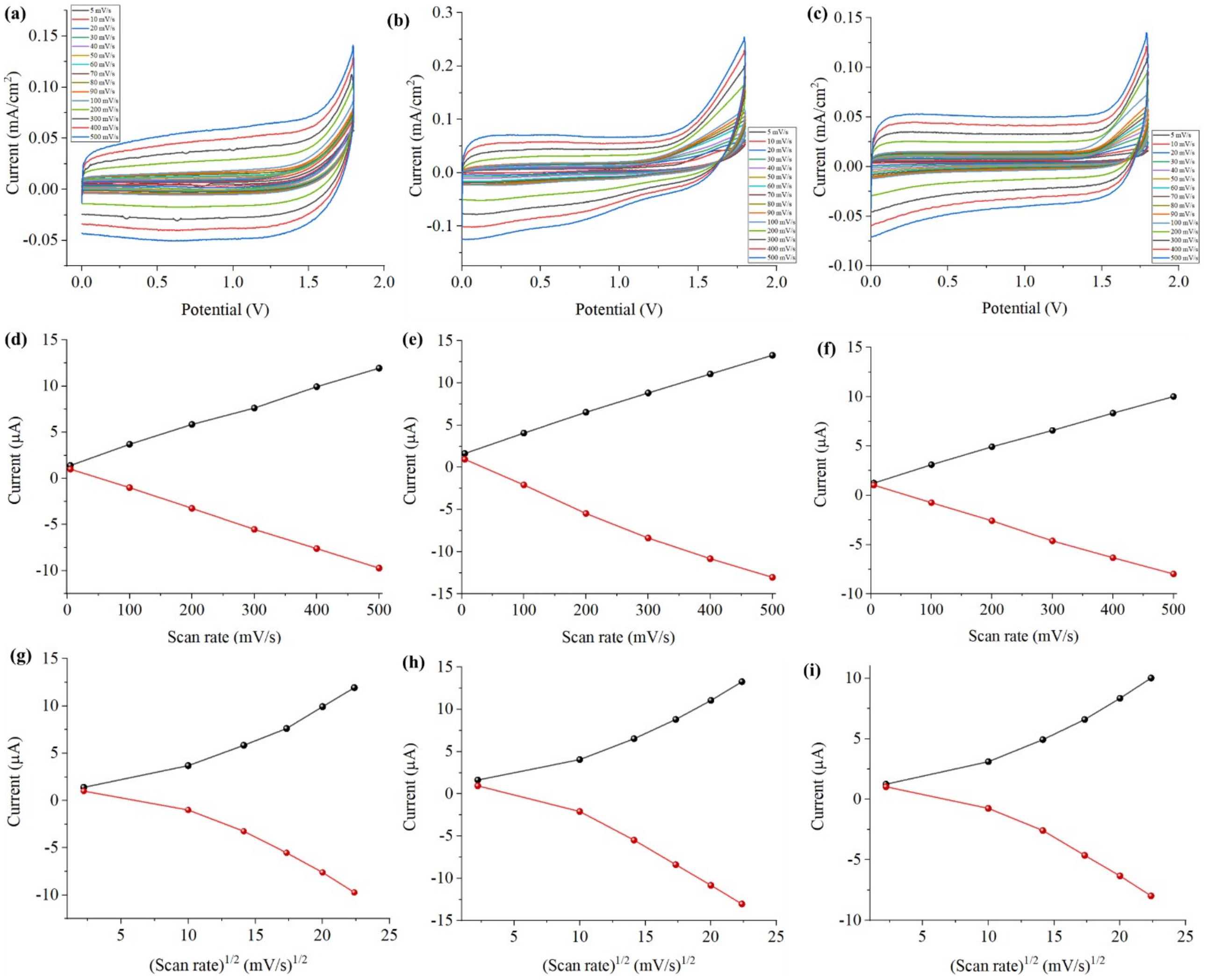

Figure S46. Cyclic Voltammogram of devices made of TBFT2 at different scan rates: a) drop cast, b) drop cast and nafion, and c) gel state. The dependence of current on the scan rates: d) drop cast, e) drop cast and nafion, and d) gel; and the square root of the scan rates: g) drop cast, h) drop cast and nafion, and i) gel.

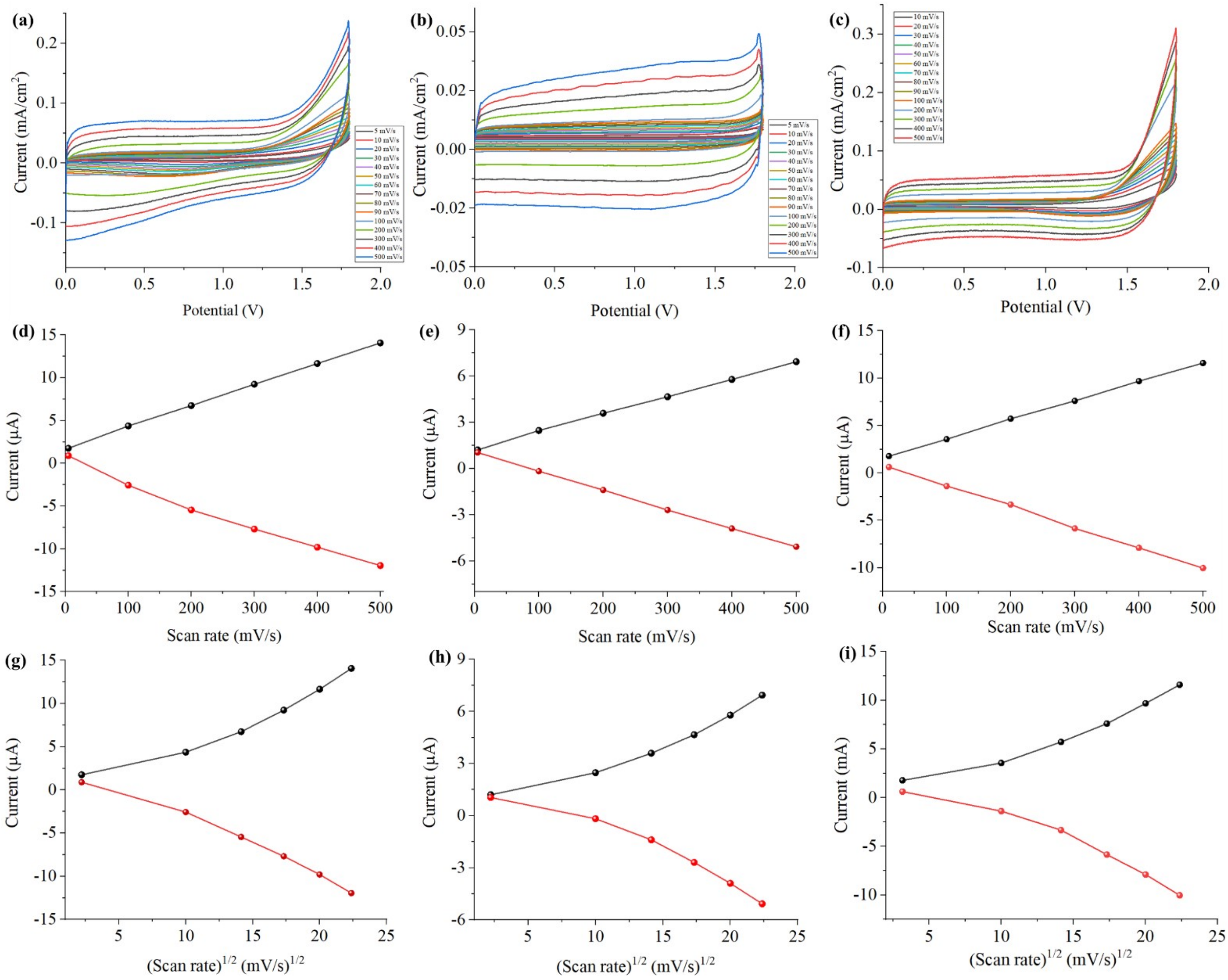

Figure S47. Cyclic Voltammogram of devices made of TBFT3 at different scan rates: a) drop cast, b) drop cast and nafion, and c) gel state. The dependence of current on the scan rates: d) drop cast, e) drop cast and nafion, and d) gel; and the square root of the scan rates: g) drop cast, h) drop cast and nafion, and i) gel.

Section M. Open circuit potential (OCP) vs. time plots of TBFT1-3

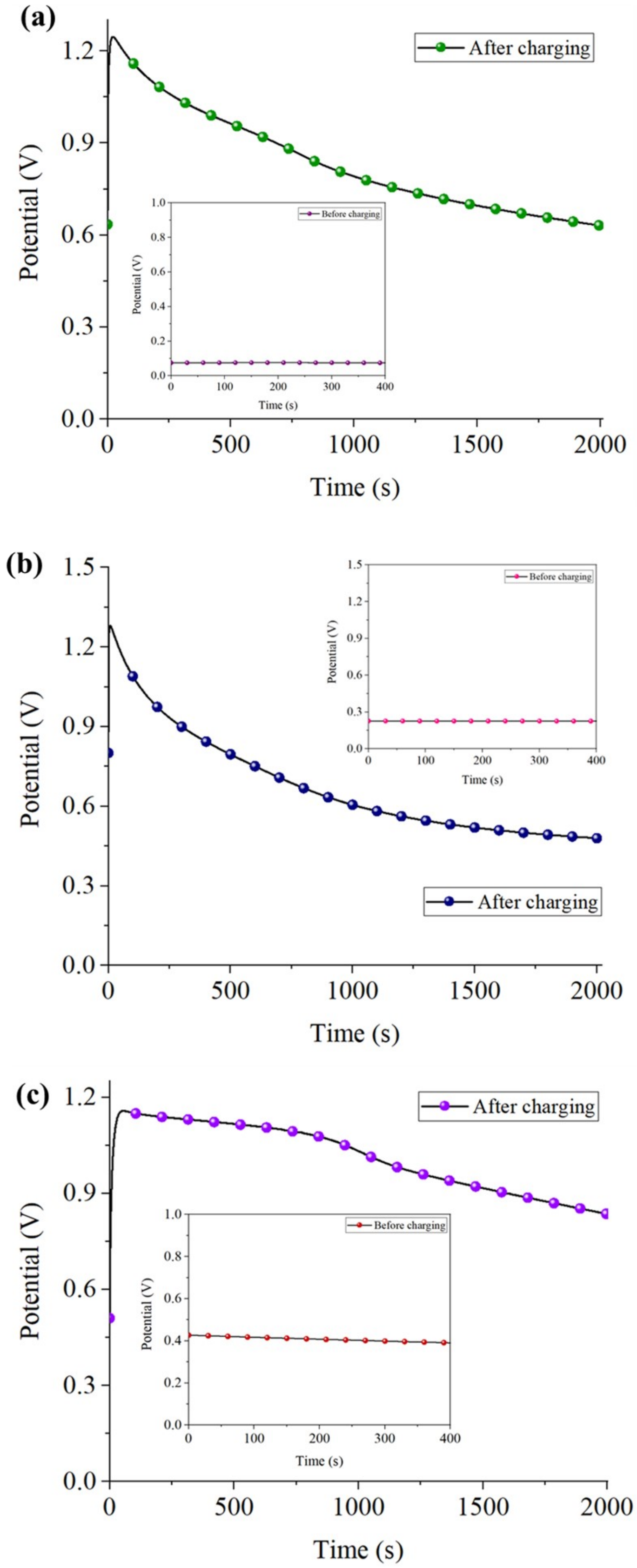

Figure S48. Open circuit potential vs. time plots of TBFT1 in a) drop cast, b) drop cast and nafion, and c) gel state.

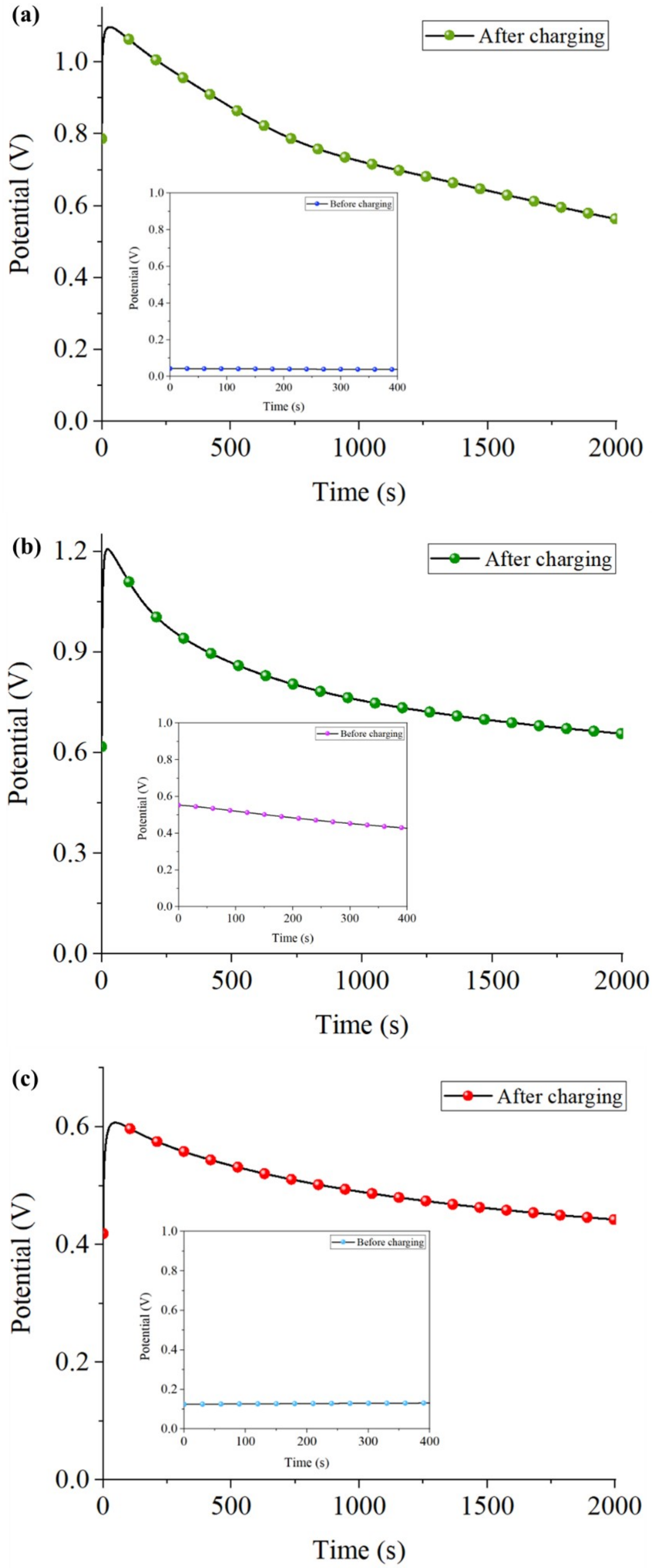

Figure S49. Open circuit potential vs. time plots of TBFT2 in a) drop cast, b) drop cast and nafion, and c) gel state.

Figure S50. Open circuit potential vs. time plots of TBFT3 in a) drop cast, b) drop cast and nafion, and c) gel state.

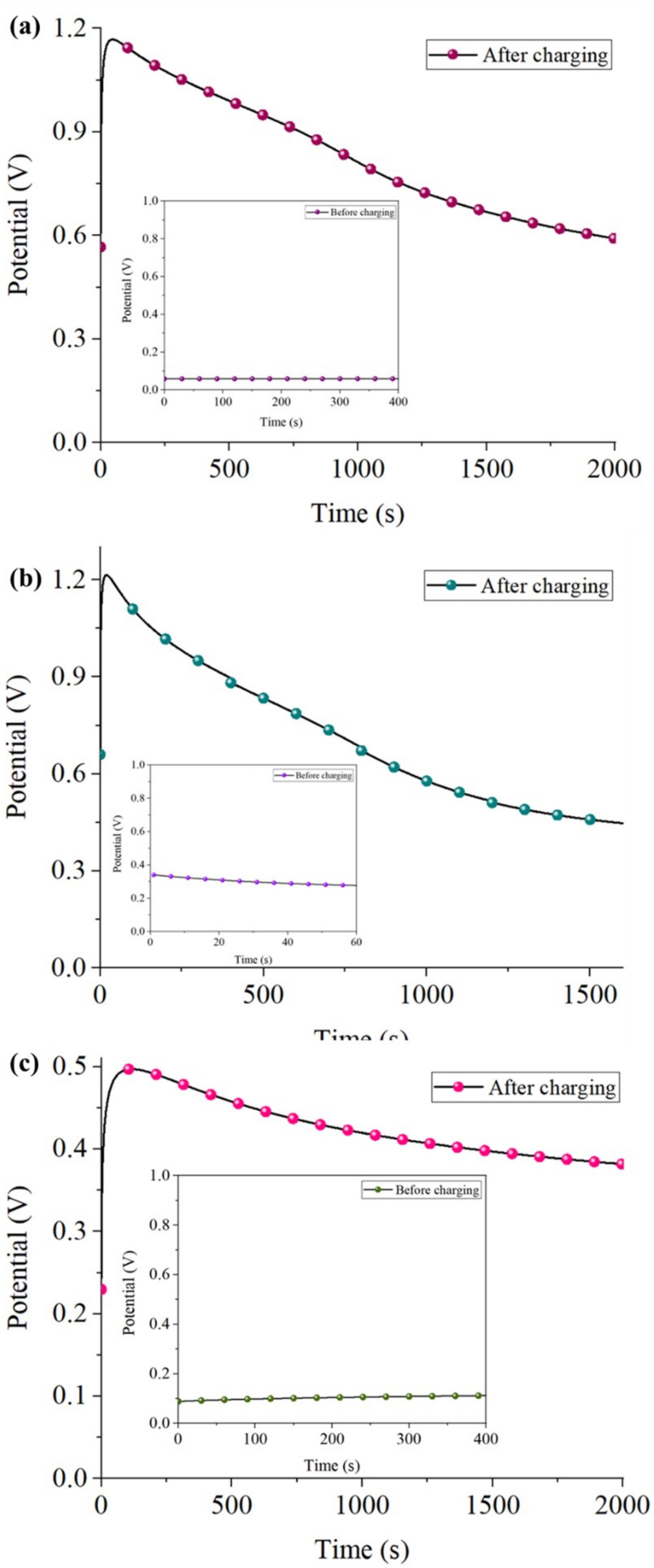

Section N. Galvanostatic Charging-discharging Cycling Stability Tests of the Devices

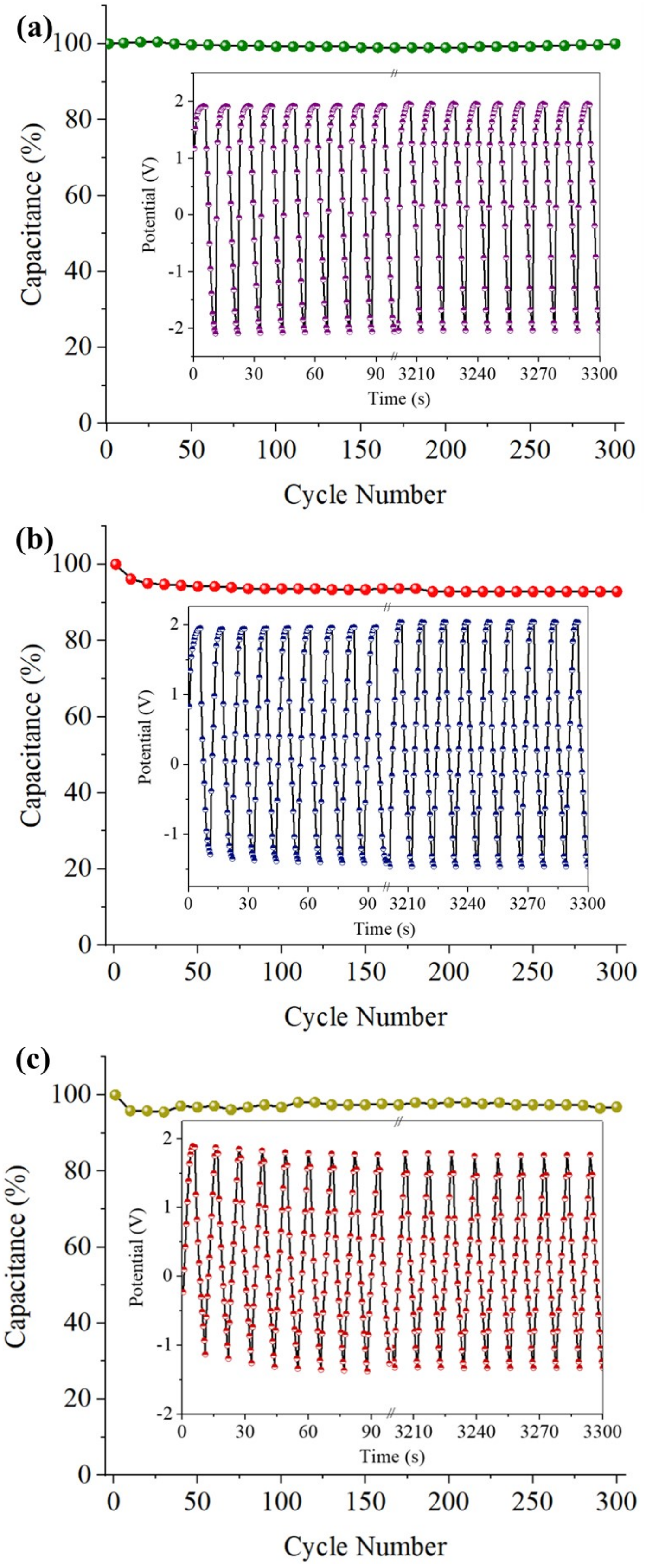

Figure S51. Cycling stability tests of the supercapacitors made of TBFT2 in a) drop cast (at c.d. 50 A/g), b) nafion coating on the drop cast layer (at c.d. 20 A/g), and c) gel state (at c.d. 10 A/g).

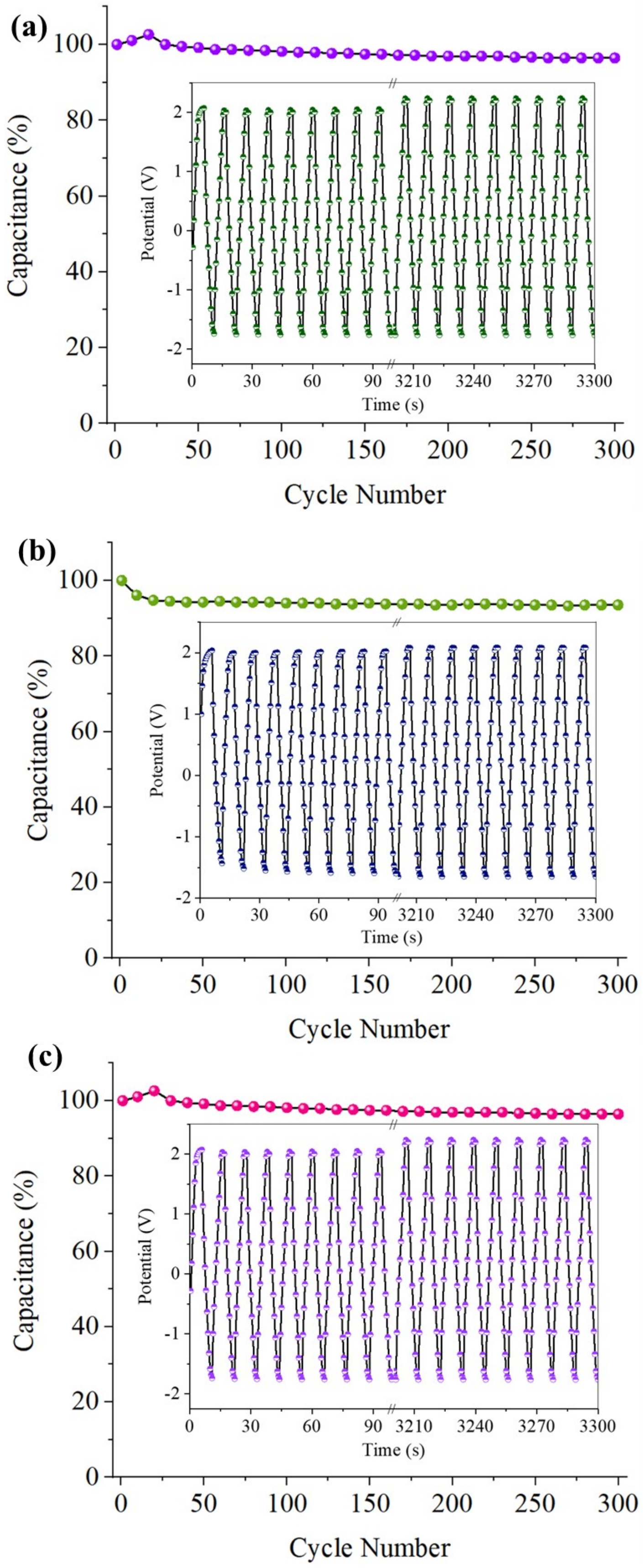

Figure S52. Cycling stability tests of the supercapacitors made of TBFT3 in a) drop cast (at c.d. 30 A/g), b) nafion coating on the drop cast layer (at c.d. 30 A/g), and c) gel state (at c.d. 20 A/g).

Section O: OCP and Specific capacitance values of TBFT1-3

Table S2. Open circuit potential (OCP) and Specific capacitance values of TBFT1-3.

Compounds		Potential (V)			Specific Capacitance (mAh/g)
		Before charging	After charging		
			0 s	2000 s	
TBFT1	Drop cast	0.07	1.24	0.63	9.48 (at c.d. 10 A/g)
	Drop cast and nafion	0.22	1.28	0.48	34.72 (at c.d. 50 A/g)
	Gel	0.42	1.15	0.83	16.05 (at c.d. 20 A/g)
TBFT2	Drop cast	0.04	1.09	0.56	33.07 (at c.d. 50 A/g)
	Drop cast and nafion	0.55	1.20	0.66	16.71 (at c.d. 20 A/g)
	Gel	0.12	0.61	0.44	8.67 (at c.d. 10 A/g)
TBFT3	Drop cast	0.06	1.17	0.59	20.09 (at c.d. 30 A/g)
	Drop cast and nafion	0.33	1.21	0.45	24.49 (at c.d. 30 A/g)
	Gel	0.1	0.49	0.38	15.09 (at c.d. 20 A/g)

Section P: References

(1) A. A. Boopathi, S. Sampath, T. Narasimhaswamy, *New J. Chem*. **2019**, *43*, 9500-9506.

(2) S. Sampath, A. A. Boopathi, A. B. Mandal, *Phys. Chem. Chem. Phys*. **2016**, *18*, 21251-21258.